

CO₂ collision-induced line parameters for the ν_3 band of ¹²CH₄ measured using a hard-collision speed-dependent line shape and the relaxation matrix formalism

T. Bertin^a, J. Vander Auwera^{a,1,*}

^a*Spectroscopy, Quantum Chemistry and Atmospheric Remote Sensing (SQUARES), C.P. 160/09, Université Libre de Bruxelles, 50 avenue F.D. Roosevelt, B-1050 Brussels, Belgium*

Abstract

Ten high resolution Fourier transform spectra of the pentad region near 3.3 μm of methane diluted in carbon dioxide at total pressures up to 800 hPa have been recorded at 296.5 (5) K. Including a high resolution spectrum of pure methane at low pressure, these spectra have been analyzed using multi-spectrum fitting techniques. The methane lines were modeled using hard-collision speed-dependent line profiles and line mixing was included in the strongest absorption regions, considering the first order Rosenkranz approximation and the relaxation matrix formalism. CO₂ broadening and shift coefficients have been measured, together with the speed dependence of broadening. Results obtained using the two line mixing models are intercompared and compared with previous work.

Keywords:

High resolution infrared spectroscopy, CO₂ broadening and shift coefficients, Speed dependence of broadening, First order line mixing, Relaxation matrix formalism

1. Introduction

Methane is rather ubiquitous in planetary atmospheres. In addition to being a strong greenhouse gas on the Earth [1], it is indeed observed in the atmospheres of the giant planets of the Solar system ([2, 3] for example), Titan [4] and exoplanets [5–7]. Although its presence in the CO₂ rich atmosphere of Mars is unclear [8], the possible contribution of CH₄-CO₂ collision induced absorption (CIA) to global warming of the atmosphere of early Mars [9] motivated recent spectroscopic investigations [10, 11]. In particular, the work of Tran *et al.* [11] was focused on the modeling of absorption spectra of the 3.3 μm region of CH₄ diluted in CO₂ at total pressures from 3 to 25 bars, recorded using Fourier transform spectroscopy. Following up on that contribution, the present work aimed to characterize the effects of sub-atmospheric CO₂ pressures on the shape of lines of the ν_3 band of ¹²CH₄, observed in that spectral range.

An extensive review of the literature reporting measurements of line shape parameters for the ν_3 band of methane can be found in [12]. Spectroscopic studies dealing with the CH₄+CO₂ system

*Corresponding author

Email address: jean.vander.auwera@ulb.be (J. Vander Auwera)

¹Senior research associate with the F.R.S.-FNRS, Belgium

are rather scarce [11–19]. They are summarized in Table 1. Using a distributed feedback diode laser spectrometer, Gharavi and Buckley [13] measured CO₂ (as well as self, N₂, CO and H₂O) pressure broadening coefficients of the R(3) and R(4) manifolds of the 2ν₃ band at 296 K and higher temperatures. The measurements were carried out using a Voigt profile, the Lorentz halfwidth of all the components of each manifold being set the same. Also using a Voigt line shape and applying a multispectrum fitting procedure to 12 high resolution Fourier transform spectra recorded at 296 K (3 spectra of pure CH₄ and 9 spectra of CH₄+CO₂ mixtures at total pressures from 22 to 759 hPa), Lyulin *et al.* [14] measured CO₂ broadening and shift coefficients for respectively 533 and 386 CH₄ lines belonging to several bands observed in the 5550 – 6140 cm^{−1} spectral range. In addition to using the Voigt line shape, other studies considered finer effects such as Dicke narrowing [20]. In particular, Fissiaux *et al.* [15] compared CO₂ broadening coefficients measured using the Voigt, Rautian and Galatry profiles for 28 lines of the ν₄ band of ¹²CH₄ observed in tunable diode laser spectra recorded at 4 total pressures between 8 and 50 hPa. Vispoel *et al.* [16] followed a similar approach for 10 lines of the ν₃ band of ¹²CH₄, relying on spectra recorded at 4 total pressures between 20 and 60 hPa. Using the Voigt and Galatry line shapes, Es-sebbar and Farooq [17] measured the intensities and CO₂ (as well as N₂, O₂, H₂, He and Ar) broadening and narrowing coefficients for 7 lines of the P(11) manifold of the ν₃ band of ¹²CH₄ observed in 10 spectra recorded at 297(1) K and total pressures up to about 100 torr using a difference frequency laser system. The CO₂ broadening coefficients are unfortunately only provided in a figure. Es-sebbar and Farooq extended these measurements to the P(5), P(7), P(9), P(10), P(12) and P(13) manifolds of the same band, relying on 8 spectra of each manifold recorded at total pressures between 10 and 201 torr [12]. The broadening coefficients and average narrowing coefficients are reported. Manne *et al.* [18] used a distributed feedback laser to record 8 spectra of the R(3) manifold of ¹²CH₄ (3 lines) and 9 spectra of the R(4) manifold of ¹³CH₄ (4 lines) perturbed by CO₂ (as well as air and He) at total pressures up to about 150 and 200 hPa, respectively. The Voigt, Rautian, Galatry and speed dependent Voigt profiles, not including or including first order line mixing [21] with the latter, were used to measure line shape parameters. Most of these are reported in figures, numerical values being only provided for the air, He and CO₂ broadening coefficients, their relative speed dependence and the first order line mixing parameters measured with the speed dependent Voigt profile with line mixing. As already mentioned above, the work of Tran *et al.* [11] was focused on the modeling of absorption spectra of the 3.3 μm region of CH₄ diluted in CO₂ at total pressures from 3 to 25 bars, relying on line shape parameters available in the HITRAN database [22]. To develop a method to determine the concentration of methane during oxy-methane combustion in a mixture of CO₂, O₂ and Ar, Koroglu *et al.* [19] measured absorption cross sections of methane mixed with each of these three gases at 296 K and atmospheric pressure in the 3.402 – 3.405 μm range using FTIR, and at two wavelengths in the P(8) manifold at temperatures from 700 to 2000 K and pressures from 0.1 to 1.5 atm using a shock tube and a distributed feedback inter-band cascade laser.

Modeling the effects of higher pressures on the infrared spectrum of methane is challenging, going beyond studies of finer pressure effects such as those referred to here above. As a result of the tetrahedral symmetry of the molecule, methane absorption bands indeed involve manifolds of closely spaced spectral lines that interact by means of inelastic collisions at higher pressures [23]. This line mixing is frequently modeled using the first order approximation [21]. However, this “weak coupling” approximation is not appropriate for pressures approaching 1 atm [24], therefore calling for the more appropriate solution relying on the relaxation matrix formalism [25, 26].

In this context, the present work aims to provide a larger set of parameters characterizing the

Table 1: Previous measurements of CO₂ collision induced parameters (“Par.”) reported for methane in the literature.

Reference	Band	Range / cm ⁻¹	# lines	Par. [†]	Line profile [‡]
Gharavi & Buckley (2005) [13]	2 ν_3	6046 – 6058	7	b_L^0	Voigt
Lyulin <i>et al.</i> (2014) [14]	2 ν_3	5550 – 6140	533	b_L^0, δ^0	Voigt
Fissiaux <i>et al.</i> (2014) [15]	ν_4	1241 – 1369	28	b_L^0	Voigt, Rautian & Galatry
Vispoel <i>et al.</i> (2019) [16]	ν_3	2906 – 2959	11	b_L^0	Voigt, Rautian & Galatry
Es-sebbar & Farooq (2014) [17]	ν_3	2905 – 2908	9	b_L^0, β^0	Voigt & Galatry
Manne <i>et al.</i> (2017) [18]	ν_3	3057 – 3058	3	b_L^0, a_w	qsdVoigt with first-order line mixing
Es-sebbar & Farooq (2021) [12]	ν_3	2884 – 2969	49	b_L^0, β^0	Voigt & Galatry

[†] b_L^0, δ^0, β^0 and a_w are the broadening, shift, narrowing and speed dependence of broadening coefficients.

[‡] “qsd” stands for “quadratic speed dependent.”

effects of the pressure of CO₂ on the 3.3 μm region of the spectrum of methane. The present measurements were performed considering hard collision Dicke narrowing and speed dependence of the broadening, both of which being included in the relaxation matrix and first order models developped by Ciurylo and Pine [27]. Comparisons of the first order approximation with the relaxation matrix formalism are presented, highlighting the limitations of each model and the differences between the retrieved parameters. Comparisons of the present measurements with previous work are presented as well when possible.

2. Experimental details

Unapodized high resolution spectra of pure methane (Fluka, purity $\geq 99.0\%$) and methane diluted in carbon dioxide (Aldrich, purity $\geq 99.8\%$) have been recorded using a Bruker IFS 120 to 125 HR upgrade Fourier transform spectrometer (FTS). The instrument was equipped with a tungsten source, a 1.15 mm entrance aperture diameter, a KBr beamsplitter, a band pass filter limiting the radiation reaching the detector to the 2550 – 3200 cm⁻¹ range and an InSb detector cooled down to 77 K. The sample was contained in a double jacketed 19.7 \pm 0.2 cm long stainless steel cell, closed by CaF₂ windows and located inside the evacuated spectrometer. The temperature of the cell was stabilized at 296.5 \pm 0.5 K using a ThermoHaake DC50/K20 thermostat and water as heat exchanger. It was measured using two TSiC 301 sensors (IST Innovative Sensor Technology; stated accuracy of ± 0.3 K in the 10 – 90 °C range) fixed on the outer cell wall. The methane and carbon dioxide pressures were measured using MKS Baratron manometers model 690A of 10 and 1000 Torr full scale ranges, respectively. Their accuracy of reading are conservatively estimated to be equal to 0.5 %. The total pressures and initial mole fractions of methane are listed in Table 2. All the interferograms were recorded with a maximum optical path difference (MOPD) of 150 cm, corresponding to an approximate spectral resolution (defined as 0.9/MOPD) of 0.006 cm⁻¹. The number of interferograms co-added to yield the spectra are also provided in Table 2. Transmittance spectra were generated using the average of two low resolution (0.1 cm⁻¹) empty cell spectra recorded just before and after the corresponding sample spectrum. They were interpolated 4 times.

Table 2: Total pressures P_{tot} , initial mole fractions of methane x in the CO₂ mixtures [$x = P(\text{CH}_4)/P_{tot}$ where $P(\text{CH}_4)$ is the methane pressure measured just after filling the cell] and number of interferograms co-added (n). The numbers between parentheses are the uncertainties on the total pressures given in the units of the last quoted digits, estimated as the sum in quadrature of half of the peak-to-peak variations of the pressures measured during the recording of the interferograms and the 0.5 % accuracy of reading of the pressure gauge. The uncertainty estimated for spectrum S1 is set to 3 % of the measured pressure to conservatively account for the fact that the measured low pressure is outside the calibrated range of the gauge [28].

#	P_{tot} / hPa	$x \times 10^3$	n
S1	0.407 (12)	1000.	320
S2	25.99 (13)	9.98	204
S3	51.18 (26)	7.34	320
S4	100.34 (50)	5.11	218
S5	201.2 (1.0)	5.00	320
S6	400.3 (2.0)	5.04	320
S7	400.6 (2.0)	3.81	320
S8	601.1 (3.0)	2.17	320
S9	601.7 (3.0)	3.06	320
S10	801.7 (4.0)	2.20	320
S11	802.8 (4.0)	2.83	320

Knowledge of the instrument line shape (ILS) characterizing the alignment of the FTS during the recording of the CH₄+CO₂ spectra is required to analyze them. The ILS was determined using a method described in another contribution [29]. Following other approaches [30, 31], it relies on high resolution spectra of molecules such as N₂O or OCS recorded at low pressure in the same instrumental conditions as the sample under study to determine the evolution with optical path difference of a so-called modulation function (η in Eq. 1 of [31]) from which the ILS in the spectral domain can be generated. A N₂O spectrum was therefore recorded for that purpose. Unfortunately, a storm broke down the compressor of the air conditioning system of the laboratory (installed on the roof of the building) after the recording of the N₂O spectrum and before the start of the measurements on the CH₄+CO₂ system. As its repairing turned out to require several months to complete, the experiments on CH₄+CO₂ were conducted without air conditioning. The resulting variations of temperature in the laboratory of about 1.5 K (peak to peak) during the recording of the interferograms did not affect the gaseous sample because the temperature of the cell was stabilized using a thermostat (see above), but had consequences on the alignment of the spectrometer. As a result, the ILS determined using N₂O did not correctly model the actual alignment of the FTS, as is shown in Fig. 1. The modulation function determined using N₂O lines was therefore modified to improve the modeling of the shapes of the isolated R(0, A_1 , 1, 3) and R(1, F_1 , 1, 10) lines of the ν_3 band of ¹²CH₄ observed in spectrum S1 (see Table 2). These lines are centered near 3028.752 and 3038.499 cm⁻¹, respectively. As done in our previous contribution on the ν_3 band

of $^{12}\text{CH}_4$ [24], the methane lines are identified with $\Delta J(J'', C'', \alpha'', \alpha')$ where J'' is the rotational quantum number of the lower level, $C'' = A_1, A_2, E, F_1$ or F_2 is its rovibrational symmetry in the molecular symmetry group $T_d(M)$ [32] and α is a label used to fully identify rotational levels within vibrational polyads [33] (α'' and α' are associated with the lower and upper levels of the transition, respectively). Although the modeling of these lines obtained using the modified modulation function is satisfactory, as also shown for $R(0, A_1, 1, 3)$ in Fig. 1, it is most probably not the best estimate of the actual ILS of the spectrometer.

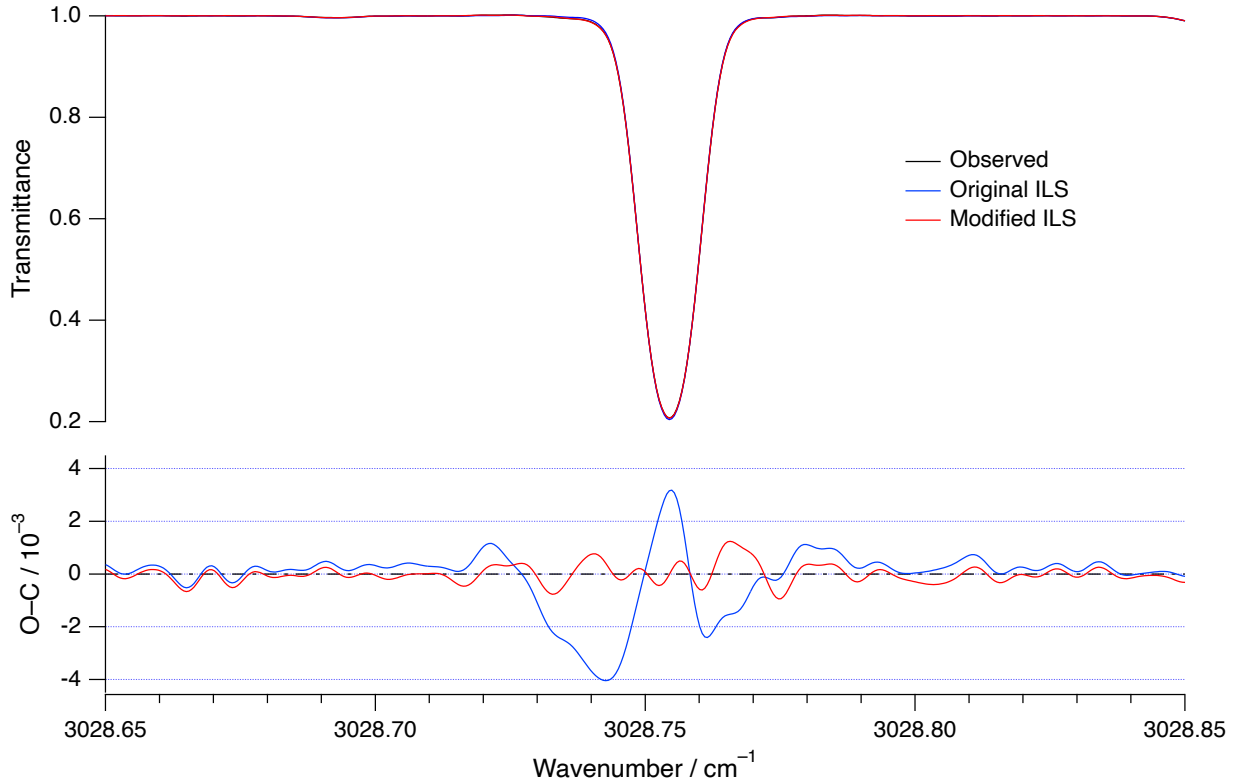


Figure 1: Least squares fit of the $R(0, A_1, 1, 3)$ line of the ν_3 band of $^{12}\text{CH}_4$ (spectrum S1 in Table 2, 296.5 K and 19.7 cm) with the ILS determined using N_2O (blue trace) and modified relying on the $R(0, A_1, 1, 3)$ and $R(1, F_1, 1, 10)$ lines observed in spectrum S1 (red trace).

3. Modeling the absorption spectra

Each of the 11 observed spectra were modeled as the convolution of the ILS with a molecular transmittance $\tau(\tilde{\nu})$ ($\tilde{\nu}$ is the wavenumber, in cm^{-1}). The molecular transmittance was generated using the following expression

$$\tau(\tilde{\nu}) = b(\tilde{\nu}) \exp \left\{ -N\ell [8\pi^3/(3hc)] \tilde{\nu} [1 - \exp\{-hc\tilde{\nu}/(k_B T)\}] F(\tilde{\nu}) \right\} \quad (1)$$

where $b(\tilde{\nu})$ is the baseline represented by a polynomial expansion, N is the density of absorbing molecules (in molecule/ cm^3), h is the Planck constant, c is the speed of light in vacuum, k_B is the Boltzmann constant, T is the temperature (in K), ℓ is the optical path length (in cm) and $F(\tilde{\nu})$ is the “spectral distribution.”

In the absence of line mixing, the contributions of the various transitions to the spectral distribution is given by [34]

$$F(\tilde{\nu}) = \sum_n \frac{1}{4\pi\varepsilon_0} \mu_n^2 \rho_n g(\tilde{\nu} - \tilde{\nu}_n) \quad (2)$$

In this expression, ε_0 is the electric constant and the index n represents a rovibrational transition corresponding to a spectral line, the summation running over all the transitions leading to lines observed in the considered spectral range. For each transition n , ρ_n is the relative population of the lower level, μ_n is the electric dipole transition moment (in D) and $g(\tilde{\nu} - \tilde{\nu}_n)$ is the line shape function centered around the wavenumber $\tilde{\nu}_n = E'_n - E''_n$ where E'_n and E''_n are the energies of the upper and lower levels, respectively. The relative population of the lower level is expressed as

$$\rho_n = g''_n \frac{\exp\{-hcE''_n/(k_BT)\}}{Q(T)} \quad (3)$$

where g''_n is the degeneracy of the lower level of the transition n and $Q(T)$ is the total internal partition sum. The latter was calculated to be equal to 592.07 and 1184.2 at 296.5 K for $^{12}\text{CH}_4$ and $^{13}\text{CH}_4$, respectively [35]. The electric dipole transition moment associated with a given transition n was obtained from the integrated absorption cross section σ_n of the corresponding line using the following relation

$$\mu_n^2 = \frac{\sigma_n}{A \tilde{\nu}_n \rho_n [1 - \exp\{-hc\tilde{\nu}_n/(k_BT)\}]} \quad (4)$$

where $A = [8\pi^3/(3hc)] \times [1/(4\pi\varepsilon_0)] \approx 4.162 \times 10^{-19} \text{ D}^{-2} \text{ cm}^2$. In the present work, the line shape function used to model the profile of the $^{12}\text{CH}_4$ lines was chosen to be the hard collision speed dependent profile introduced by Lance *et al.* [36] because it minimized the residuals obtained for the isolated R(0, A_1 , 1, 3) and R(1, F_1 , 1, 10) lines, as shown in Fig. 2. This observation is partially supported by previous work in which narrowing [12, 16, 17], speed dependence [18] or both effects [37] were included for CO_2 or other buffer gases. Hard collisions were considered because CO_2 is almost three times as heavy as methane. The hard collision speed dependent profile was computed in its quadratic speed dependence approximation [38] using the FORTRAN routine “qSDHC.for” [39]. Although it has more physical foundation, the hypergeometric speed dependence model was not considered because it did not improve the residuals but significantly increased computation time. The correlation between velocity- and phase-changing collisions was neglected for the same reason. The three other line shape models considered in Fig. 2 were computed as follows. The quadratic speed dependent Voigt line shape was calculated using the routine “qSDV.for” from Tran *et al.* [39], while the Voigt and Rautian profiles were computed using the complex probability (or error) function (see Eq. 4 of [24] for example) calculated using the weideman40a() function provided in the “Py4CATS” package [40]. The shape of the weaker $^{13}\text{CH}_4$ lines was modeled with a Voigt profile or a quadratic speed dependent Voigt profile with fixed speed dependence of the broadening (see below).

In addition to its position $\tilde{\nu}_n$, the hard collision speed dependent profile used to describe the shape of each $^{12}\text{CH}_4$ line n involves 3 parameters. They are the speed dependent line broadening $\Gamma_n(v)$ (v is the absolute speed of the absorbing molecule), the line shift Δ_n and the line narrowing β_n . These 3 parameters are in cm^{-1} . Their dependence with pressure, including the speed dependence of the line broadening expressed by the coefficient a_w [37, 41], was modeled according to:

$$\Gamma_n(v) = P_{tot} [b_L^0(\text{CO}_2)(1 - x) + b_L^0(\text{self})x] \times \left[1 + a_w \left(\frac{v^2}{v_p^2} - \frac{3}{2} \right) \right] \quad (5)$$

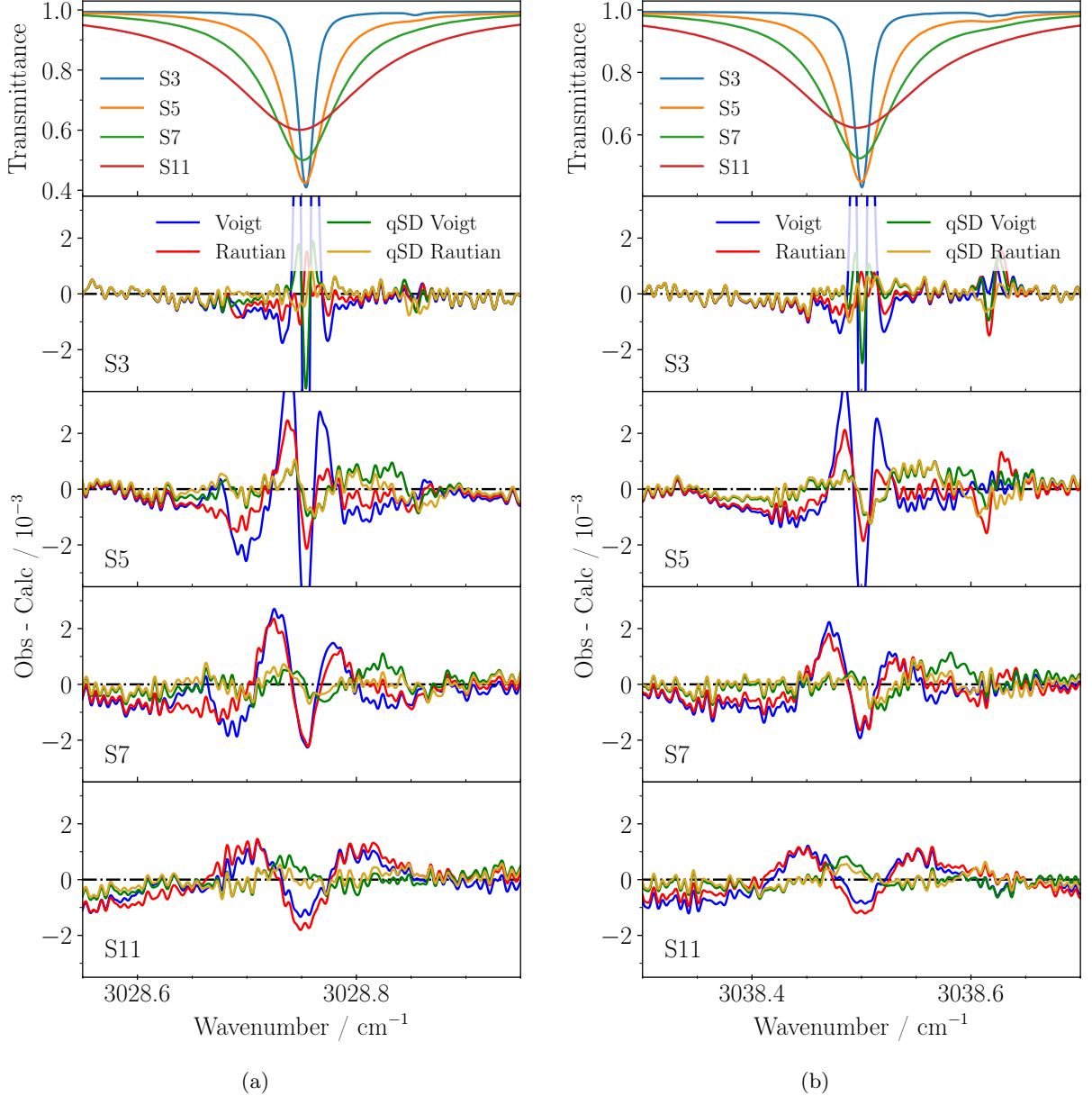


Figure 2: Results of the fit of the $R(0, A_1, 1, 3)$ (left) and $R(1, F_1, 1, 10)$ (right) lines of the ν_3 band of $^{12}\text{CH}_4$ perturbed by CO_2 using 4 different theoretical line shape models (“qSD” stands for “quadratic speed dependent”). Four of the 11 transmittance spectra measured are presented in the top row (296.5 K and 19.7 cm; the pressures and mole fractions are provided in Table 2). The best-fit residuals obtained for the 4 spectra of the two lines are presented in the lower 4 rows, the color of each trace being associated with a specific line shape model.

$$\Delta_n = P_{tot} [\delta^0(\text{CO}_2)(1 - x) + \delta^0(\text{self}) x] \quad (6)$$

$$\beta_n = \beta^0 P_{tot} \quad (7)$$

where $x = P(\text{CH}_4)/P_{tot}$ is the methane mole fraction, P_{tot} is the total pressure (in atm), v_p is

the most probable speed of the methane molecules, and $b_L^0(\text{CO}_2)$, $b_L^0(\text{self})$, $\delta^0(\text{CO}_2)$, $\delta^0(\text{self})$ and β^0 are the CO_2 broadening, self broadening, CO_2 shift, self shift and narrowing coefficients (in $\text{cm}^{-1}\text{atm}^{-1}$) of the methane lines, respectively. As it is defined in Eq. 5, the speed dependence of the line broadening a_w is unitless and is assumed to be the same for CO_2 and self broadening. Narrowing is also assumed to be independent of the broadening gas.

At higher pressures, observed spectra can *a priori* not be modeled by the sum of isolated lines anymore because of the rise of collisional line mixing effects [23]. The use of Eq. 2 would indeed lead to characteristic signatures in the residuals [34]. Several models of these effects exist [21, 23, 25, 27, 42–47]. Within the Rosenkranz first order approximation [21], Eq. 2 can still be used to model observed spectra with the line shape function involved given by [48–50]

$$g_{lm}^n(\tilde{\nu} - \tilde{\nu}_n) = \text{Re}\{w(\tilde{\nu} - \tilde{\nu}_n)\} + Y_n^0 P_{tot} \text{Im}\{w(\tilde{\nu} - \tilde{\nu}_n)\} \quad (8)$$

where $w(\tilde{\nu} - \tilde{\nu}_n)$ is the complex normalized spectral shape of the isolated line, its real ($\text{Re}\{\cdot\}$) and imaginary ($\text{Im}\{\cdot\}$) parts being conveniently provided by the routines “**qSDHC.for**” and “**qSDV.for**” [39] for the quadratic speed dependent hard collision (*i.e.* Rautian) and Voigt profiles, respectively. Y_n^0 (in atm^{-1}) is the first order line mixing parameter, expressing the coupling of line n with neighboring lines. This approach has drawbacks [34] and is *a priori* limited to weak line coupling and small overlapping. Ciuryło and Pine [27] derived a general form of the spectral distribution for hard collision speed dependent profiles affected by line mixing:

$$\begin{aligned} F(\tilde{\nu}) &= \frac{1}{\pi} \text{Re}\left\{ \boldsymbol{\mu}^T [\mathbf{1} - \mathbf{G}(\tilde{\nu})\boldsymbol{\beta}]^{-1} \mathbf{G}(\tilde{\nu}) \boldsymbol{\rho} \boldsymbol{\mu} \right\} \\ \mathbf{G}(\tilde{\nu}) &= \int f_M(\mathbf{v}) \times \left[\mathbf{W}(\mathbf{v}) + \boldsymbol{\beta} - i\tilde{\nu}\mathbf{1} + i\tilde{\nu}_0 + \frac{i}{2\pi c} (\mathbf{k}^T \mathbf{v}) \mathbf{1} \right]^{-1} d^3 \mathbf{v} \end{aligned} \quad (9)$$

Considering that N lines are involved, $\mathbf{G}(\tilde{\nu})$ is a $N \times N$ matrix, $\boldsymbol{\mu}$ is a N -dimensional vector of the electric dipole transition moments, $\mathbf{1}$ is the $N \times N$ unit matrix and $\tilde{\nu}_0$, $\boldsymbol{\rho}$ and $\boldsymbol{\beta}$ are $N \times N$ diagonal matrices of the line centers, relative populations ($\rho_{nn} = \rho_n$ given in Eq. 3) and narrowing parameters ($\beta_{nn} = \beta_n$ given in Eq. 7), respectively. $\boldsymbol{\rho}$ and $\boldsymbol{\beta}$ are considered to be speed independent [51]. \mathbf{k} is the N -dimensional wave vector of amplitude $|\mathbf{k}| = 2\pi\tilde{\nu}$, \mathbf{v} is a N -dimensional vector of the absolute velocity of the absorbing molecule and \mathbf{W} is the $N \times N$ relaxation matrix. Its diagonal elements are equal to $\mathbf{W}_{nn} = \Gamma_n(v) + i\Delta_n$, where $\Gamma_n(v)$ and Δ_n are as given in Eqs. 5 and 6, respectively. Its off-diagonal elements are $\mathbf{W}_{mn} = -W_{mn}P_{tot}$, where W_{mn} is the speed independent line mixing parameter that characterizes the coupling between lines n and m . The off-diagonal elements are connected by the detailed balance equation, *i.e.* $W_{mn}\rho_n = W_{nm}\rho_m$ [34]. All the elements of \mathbf{W} are in cm^{-1} . $f_M(\mathbf{v})$ is the Maxwell-Boltzmann velocity distribution [27]. The first-order line-mixing parameters Y_n^0 introduced in Eq. 8 are related to the off-diagonal elements of the relaxation matrix by [48]:

$$Y_n^0 = 2 \sum_{m \neq n} \frac{\mu_m}{\mu_n} \frac{\mathbf{W}_{mn}}{\tilde{\nu}_n - \tilde{\nu}_m} \quad (10)$$

To analyze the recorded spectra in the first order line mixing approximation (Eqs. 1, 2 and 8), the multi-spectrum analysis software [52, 53] already used to study the spectra of the ν_3 band of methane perturbed by air [24] was used. A multi-spectrum analysis software was specifically developed during this work (<https://github.com/TBSpectroscopy/rm-fit>) to analyze the recorded spectra

using the relaxation matrix formalism (Eqs. 1 and 9). The program implements a Trust Region Reflective least squares fitting algorithm to adjust a synthetic spectrum to each of the 11 observed spectra, relying on the function `least_squares()` provided in the `optimize` package of the SciPy library (<https://scipy.org>) [54]. Mostly written in Python, the software relies on the FORTRAN and Python routines mentioned above to generate the line shapes [39, 40] and the Eigen C++ library (<https://eigen.tuxfamily.org>) to perform the matrix operations.

4. Analysis

The multispectrum analysis of the measured spectra S1 to S11 was carried out in the range $2880 - 3150 \text{ cm}^{-1}$, considering lines of $^{12}\text{CH}_4$ stronger than $10^{-23} \text{ cm}^{-1}/(\text{molecule cm}^{-2})$ at 296 K. These lines belong to the ν_3 , $\nu_2 + \nu_4$, $2\nu_2$ and $\nu_3 + \nu_4 - \nu_4$ bands. Lines of $^{13}\text{CH}_4$ were also included when observed. As absorption of water vapor present in the evacuated spectrometer was observed in the spectra, 77 lines of H_2^{16}O stronger than $10^{-22} \text{ cm}^{-1}/(\text{molecule cm}^{-2})$ at 296 K had to be included in the range $2966 - 3150 \text{ cm}^{-1}$. A Voigt function was used to model the shape of the $^{13}\text{CH}_4$ and H_2^{16}O lines, the parameters of which being taken from the HITRAN database [22] (downloaded from <https://hitran.org> in February 2021). The CO_2 broadening and shift coefficients of the stronger $^{13}\text{CH}_4$ lines were fitted when needed. They were otherwise left fixed to their air counterparts.

As is apparent from section 3, the modeling of each $^{12}\text{CH}_4$ line required 8 parameters, *i.e.* $\tilde{\nu}_n$, σ_n or μ_n , $b_L^0(\text{CO}_2)$, $b_L^0(\text{self})$, $\delta^0(\text{CO}_2)$, $\delta^0(\text{self})$, β^0 and a_w . Inclusion of first order line mixing added the Y_n^0 parameter, while use of the relaxation matrix formalism resulted in the addition of speed independent off-diagonal elements W_{mn} , the number of which depended upon the number of interacting lines involved in the considered spectral range. Line mixing couples lines of the same A , E and F symmetry [49]. This selection rule was explicitly taken into account in the relaxation matrix formalism, but could not in the first order approximation because the corresponding program did not allow enforcing it [24]. Coupling between the same $1 \leftrightarrow 1$ or $2 \leftrightarrow 2$ symmetries ($A_2 \leftrightarrow A_2$ for example) was considered despite the fact that it is known to be small [55, 56]. In the present work, line mixing was only considered for lines of the ν_3 band of $^{12}\text{CH}_4$.

The positions $\tilde{\nu}_n$, intensities σ_n , assignments, air broadening $b_L^0(\text{air})$ and air shift $\delta^0(\text{air})$ coefficients of the $^{12}\text{CH}_4$ lines were taken from the HITRAN database [22] (downloaded from <https://hitran.org> in December 2021). When fixed, $b_L^0(\text{CO}_2)$ and $\delta^0(\text{CO}_2)$ were therefore assumed to be equal to their air counterparts. As in [11], $b_L^0(\text{CO}_2)$ could have been set to $1.3 \times b_L^0(\text{air})$. The spectrum of the strongest methane line the CO_2 broadening of which was set to the air broadening available in HITRAN in the present work was calculated at the lowest and highest total pressures (S2 and S11 in Table 2), with $b_L^0(\text{CO}_2)$ set to $b_L^0(\text{air})$ (spectra identified as $S_{\text{calc}}^{1.0}$ hereafter) and $1.3 \times b_L^0(\text{air})$ (spectra identified as $S_{\text{calc}}^{1.3}$ hereafter). The peak amplitudes of the two ratios $S_{\text{calc}}^{1.3}/S_{\text{calc}}^{1.0}$ are smaller (lowest total pressure) or similar (highest total pressure) to the noise level observed in the residuals presented in Figs. 3 to 6. Therefore, the impact on the reported results of fixing the CO_2 broadening of the weak lines to the air broadening available in HITRAN is believed to be very small if not negligible. The self broadening and self shift coefficients of the $^{12}\text{CH}_4$ lines were fixed to the values obtained as follows. The self broadening coefficients measured using a Voigt profile for several bands of $^{12}\text{CH}_4$ [58–63] were fitted to $b_L^0(\text{self}) = \exp\{a + b m^2 + c |m|^3 + d m^4\}$ where a , b , c and d were adjustable parameters and $m = -J''$, J'' and $J'' + 1$ for P, Q and R branch lines, respectively. Separate fits were performed for lines originating from levels with the A_1 , A_2 , F_1 , F_2 and E symmetries. As the self broadening coefficients calculated for the A_1 , A_2 ,

F_1 and F_2 symmetries with the fitted values of the a , b , c and d parameters were within $\pm 2\%$ of their averages, only these averages were considered. The two sets of calculated self broadening coefficients thus determined are listed in Table 3. The self shift coefficient of all the methane lines

Table 3: Values of the self broadening coefficients determined through fits of literature data [58–63] (see text for details). $m = -J''$, J'' and $J'' + 1$ for P, Q and R branch lines, respectively. “Unc” are the standard deviations, expressed as a percentage of the corresponding values.

$ m $	$A \& F$	Unc	E	Unc
1	0.0812	6.0	0.0791	8.2
2	0.0812	6.0	0.0790	8.2
3	0.0811	6.0	0.0786	8.2
4	0.0807	6.0	0.0779	8.3
5	0.0800	6.1	0.0769	8.4
6	0.0789	6.2	0.0755	8.6
7	0.0775	6.3	0.0737	8.8
8	0.0758	6.4	0.0715	9.0
9	0.0736	6.6	0.0691	9.4
10	0.0712	6.8	0.0665	9.7
11	0.0686	7.1	0.0637	10.
12	0.0659	7.4	0.0609	11.
13	0.0630	7.7	0.0582	11.
14	0.0602	8.1	0.0557	12.
15	0.0575	8.5	0.0535	12.
16	0.0551	8.8	0.0516	13.
17	0.0529	9.2	0.0503	13.
18	0.0510	9.5	0.0495	13.
19	0.0497	9.8	0.0494	13.

considered was fixed to $\delta^0(\text{self}) = -0.0090(13) \text{ cm}^{-1}\text{atm}^{-1}$. This value is the average of the 66 self shift coefficients measured at 296 K by Pine [37] in the Q branch of the ν_3 band of $^{12}\text{CH}_4$ ($J = 1$ to 13) using a Rautian line shape with first order line mixing, each value being weighted with the square of the inverse of its uncertainty of measurement. Three of the 4 self broadening coefficients measured in the R branch of the $\nu_2 + \nu_4$ band of $^{12}\text{CH}_4$ by Mondelain *et al.* [64] agree with this average within experimental uncertainties. The parameters β^0 , Y_n^0 and W_{mn} for $m \neq n$ were set to zero when not fitted. The same applies to a_W , except for fits F3 and F4 (see below). In addition to the line parameters, one (P and R branches) to three (Q branch) baseline [$b(\tilde{\nu})$ in Eq. 1] parameters were fitted for each spectrum included in the analysis, together with the methane mole fraction $x = P(\text{CH}_4)/P_{\text{tot}}$ associated with spectra S2 to S11.

The multispectrum analysis of the measured spectra was carried out 4 different ways, identified

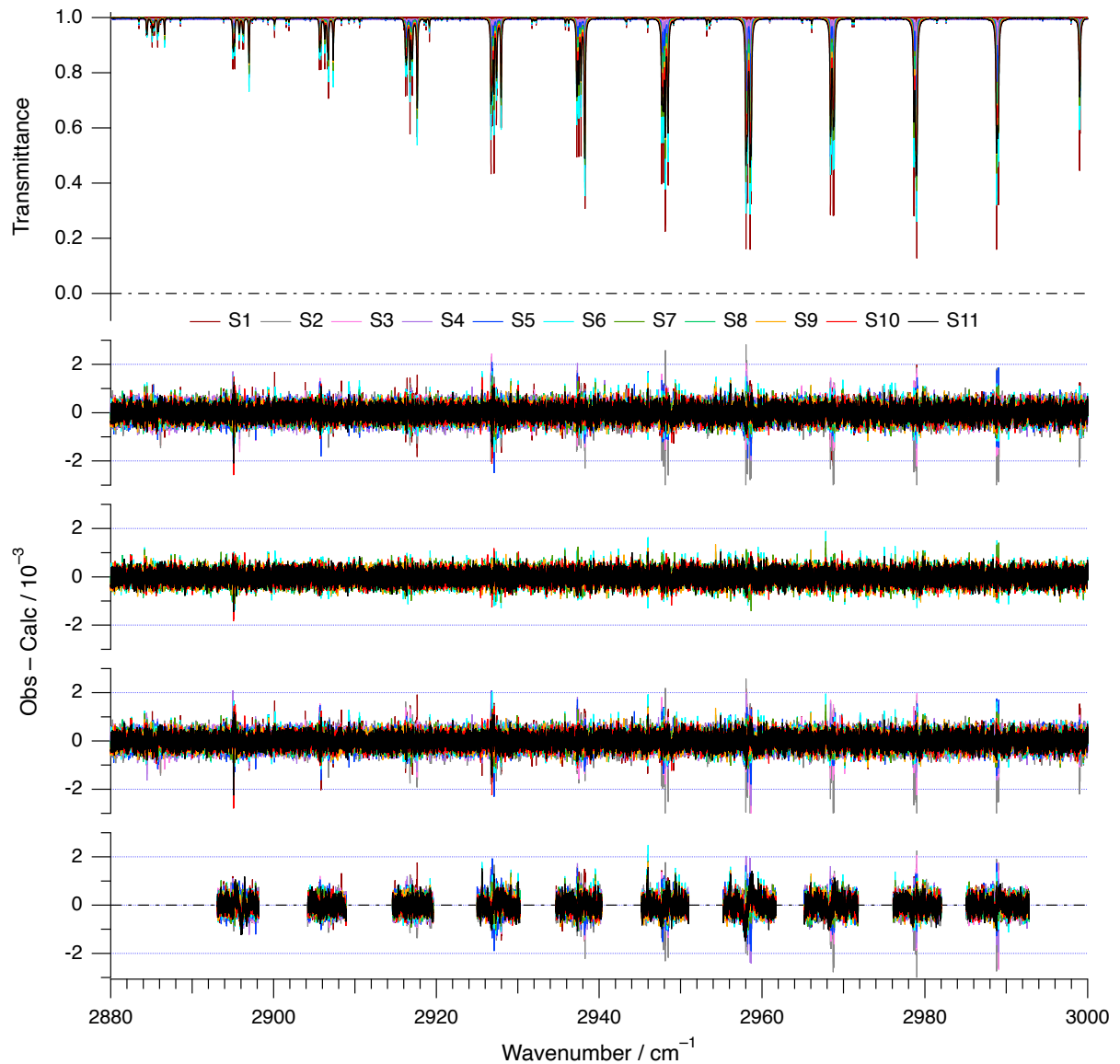


Figure 3: Transmittance spectra of the P branch of the ν_3 band of methane (top panel) and corresponding residuals obtained for the fits F1, F2, F3 and F4 (from top to bottom).

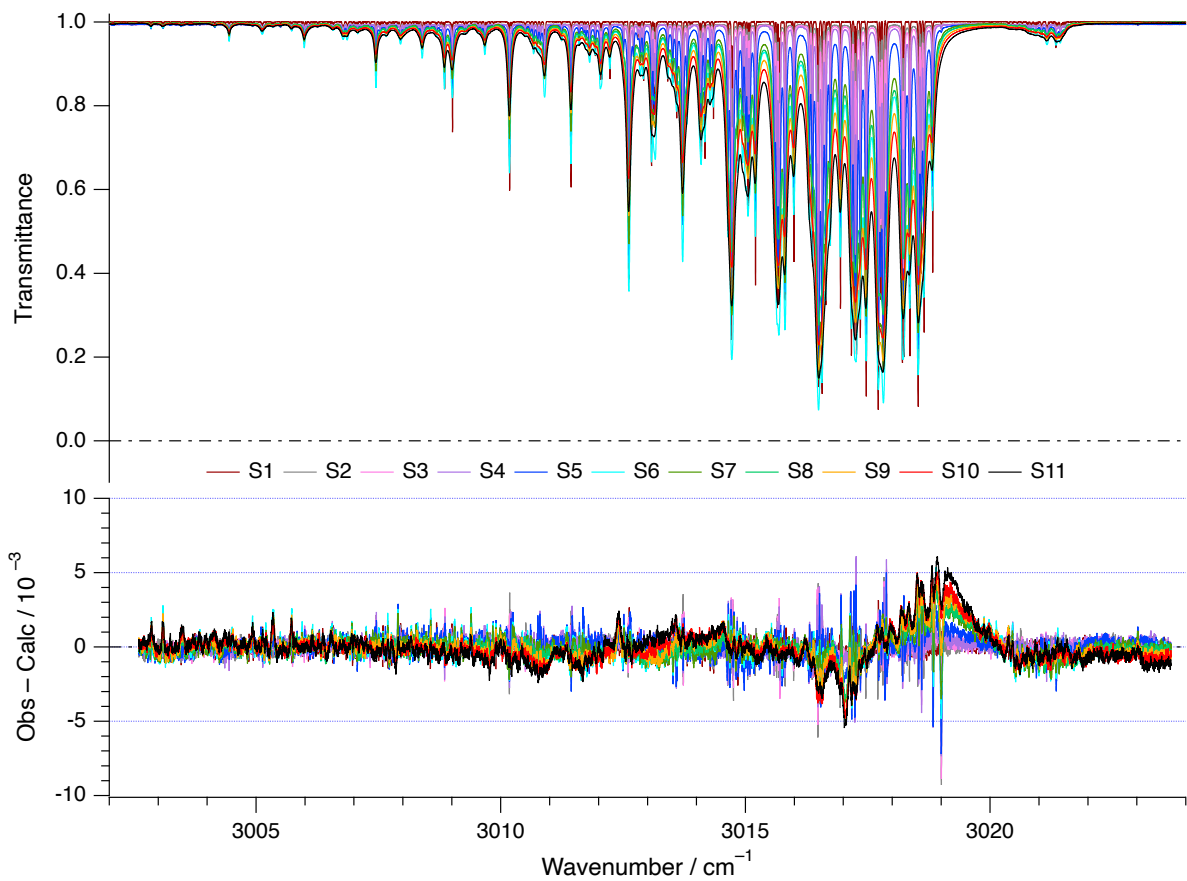


Figure 4: Transmittance spectra of the Q branch of the ν_3 band of methane (top panel) and corresponding residuals obtained for fit F4.

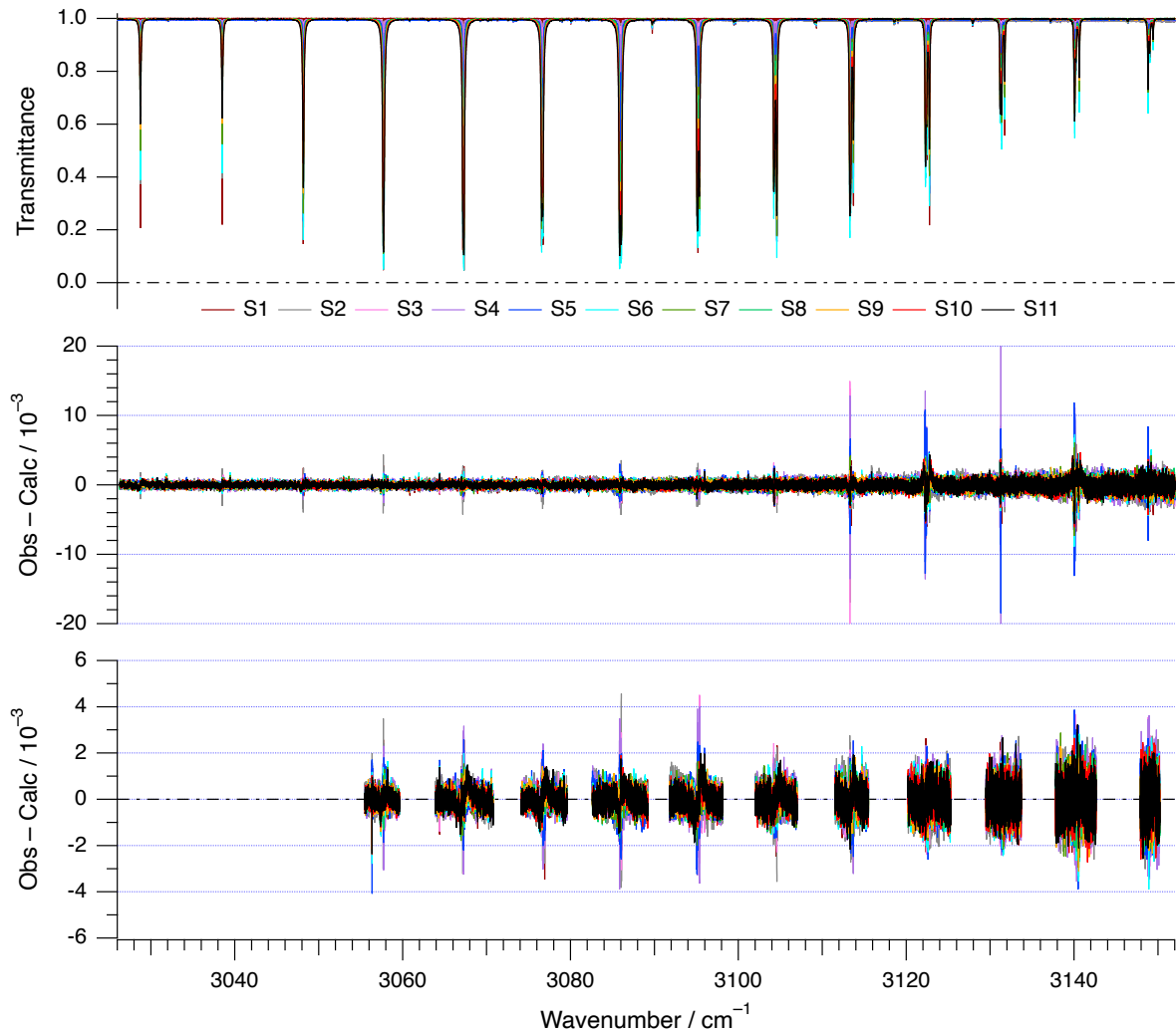


Figure 5: Transmittance spectra of the R branch of the ν_3 band of methane (top panel) and corresponding residuals obtained for the fits F1 (middle panel) and F4 (bottom panel).

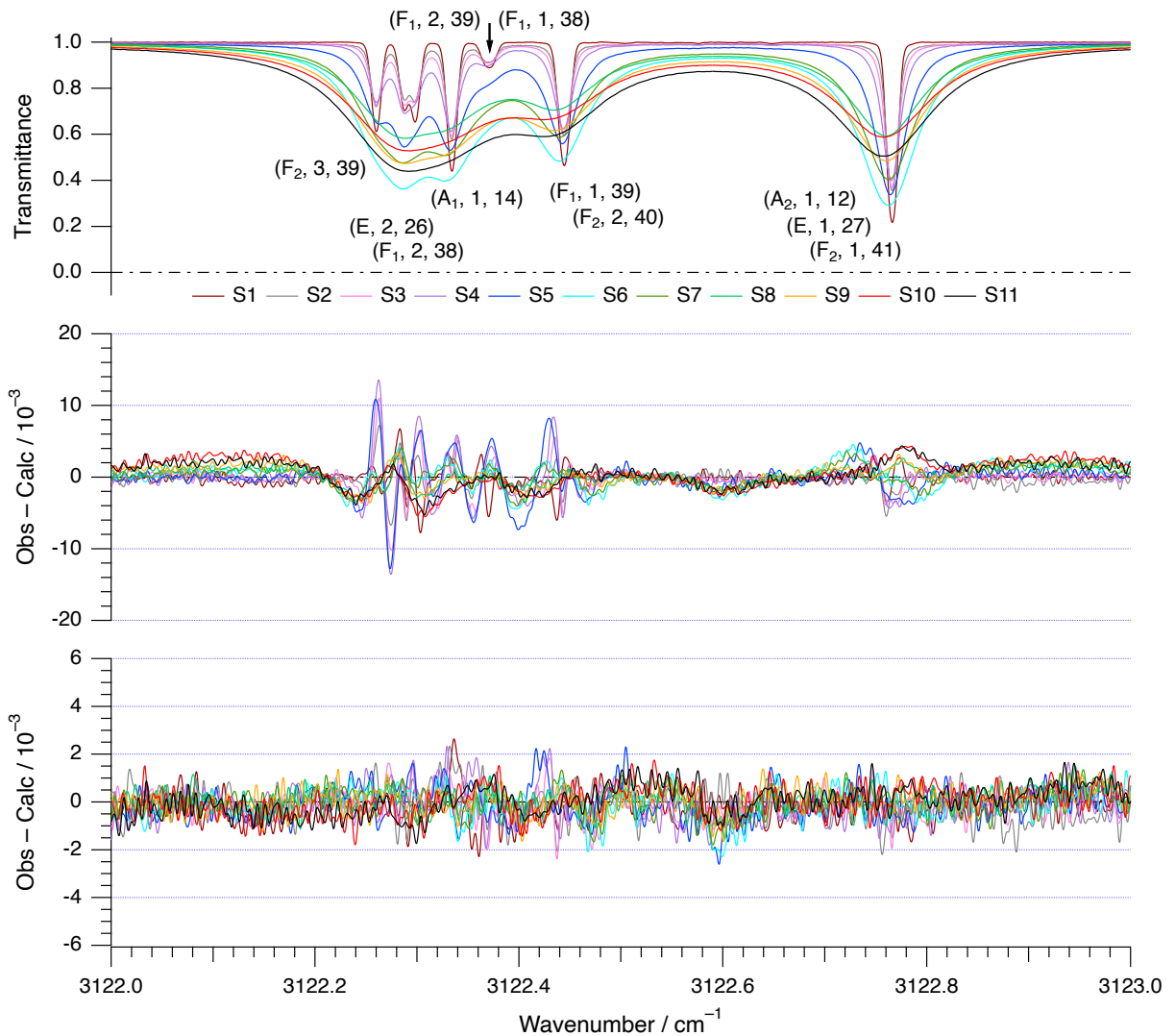


Figure 6: Same as Fig. 5, showing the R(10) manifold. In the upper panel, the lines are identified with (C'', α'', α') (see text for the meaning of the symbols).

as fits F1 to F4 from now on. The first 3 fits relied on the weak line mixing first order approximation (Eq. 8), while fit F4 relied on the relaxation matrix formalism (Eq. 9). Table 4 provides an overview of the 4 fits. Note that the parameters of a limited number of lines indicated as “fixed” in this Table were actually fitted to improve the residuals. As mentioned in the introduction, this

Table 4: Summary of the 4 fits (F1 to F4) applied to analyze the 11 spectra of Table 2. Fits F1, F3 and F4 included the 11 spectra listed in Table 2, while fit F2 considered only spectra S6 to S11. The branches studied in each fit are indicated in the second header row of columns “F1” to “F4.” The observed line shapes were modeled using the quadratic speed dependent Rautian profile. Line mixing was modeled using the first order approximation (fits F1 to F3) or the relaxation matrix formalism (fit F4). I is the line intensity in $\text{cm}^{-1}/(\text{molecule cm}^{-2})$ at 296 K; only lines with $I > 10^{-23}$ were considered. In the first three rows of columns “F1” to “F4,” the number of lines with at least one fitted parameter is given first, followed by the count of lines without fitted parameters.

$^{12}\text{CH}_4$ line parameters	F1 P & R	F2 P	F3 P	F4 P, Q & R
$I < 5 \times 10^{-22}$	138/2147	79/975	80/974	61/1598
$5 \times 10^{-22} \leq I < 5 \times 10^{-21}$	239/1	100/0	100/0	173/1
$I \geq 5 \times 10^{-21}$	147/3	70/0	70/0	213/2
$b_L^0(\text{CO}_2)^\dagger$	fit/ $b_L^0(\text{air})$	fit/ $b_L^0(\text{air})$	fit/ $b_L^0(\text{air})$	fit/ $b_L^0(\text{air})$
$\delta^0(\text{CO}_2)^\dagger$	fit/ $\delta^0(\text{air})$	fit/ $\delta^0(\text{air})$	fit/ $\delta^0(\text{air})$	fit/ $\delta^0(\text{air})$
Y_n^0 or W_{mn} \ddagger	fit/0	fit/0	fit/0	fit/0
β^0 \ddagger	fit/0	0/0	fit/0	fit/0
a_w \ddagger	fit/0	fit/0	0.110/0.110	fit/0.110

† “fit” applies to all the fitted lines.

‡ “fit” only applies to $^{12}\text{CH}_4$ lines with $I \geq 5 \times 10^{-21}$; Y_n^0 or W_{mn} were non zero for the ν_3 band only.

work aimed to analyze spectra recorded at total pressures approaching 1 atm using the relaxation matrix formalism (*i.e.* “fit F4”), more appropriate than the first order line mixing approximation. However, the spectra were also analyzed using the latter (identified as “fit F1”), as it made it possible to compare both approaches and results of this work with literature. This work actually started with fit F1. These measurements showed that the speed dependence of line broadening a_w did not exhibit a rotational dependence (see below). To determine an average value of a_w without “interferences” from Dicke narrowing, “fit F2” was performed relying on spectra involving total pressures larger than 400 hPa to allow use of the speed dependent Voigt line shape model. Fit F2 was also limited to the P branch as it is less congested and first order line mixing applies. In “fit F3,” the P branch was remeasured using the same line shape as fits F1 and F4, *i.e.* the speed dependent hard collision profile, with a_w fixed to the average value obtained in fit F2 to check its impact on the measured line shape parameters. In all fits, the J'' manifolds in the P and R branches were measured individually as they are well separated from each other. The couplings of lines involving different J levels were therefore ignored in these branches. Because of its high line density, the Q

branch was only analyzed in its entirety, in the range $3002.6 - 3023.7 \text{ cm}^{-1}$, using the relaxation matrix formalism (fit F4). To avoid having to deal with large matrices, lines separated by more than 1 cm^{-1} were considered to not be coupled and inter- J couplings were limited to $\Delta J = \pm 1$ and $J \leq 4$. The first restriction was quite effective at reducing the sizes of the matrices and prevented unrealistically large line mixing parameters. The second restriction is justified by the increase of the energy gap separating rotational levels, larger than 50 cm^{-1} between $J = 4$ and $J = 5$.

The lack of calibration of the wavenumber scales of the spectra was accounted for by multiplying the line positions read from HITRAN by the factor $(1 + C)$. In fits F1 to F3, the positions of the lines in all the analyzed manifolds of the P and R branches were kept fixed to the HITRAN values and C was fitted. For fit F4, C was only fitted for the P(8) to P(12), Q(8) to Q(13) and R(0) to R(8) manifolds of the ν_3 band, involving line positions measured using sub-Doppler spectroscopy [57]. The other manifolds were then measured with C set to the average of the values thus obtained, fitting the line positions. This “calibration” was possible because the 11 spectra were recorded one after the other, with the same instrumental conditions. During the analysis, some of the line positions available in HITRAN were found to be off by a few 10^{-2} cm^{-1} and therefore fitted. In the Q branch, line positions were determined in a separate fit of spectrum S1. Note that there seems to be a typo in the position of the R(4, A_1 , 1, 7) line provided in HITRAN as it reads $3067.300026 \text{ cm}^{-1}$ instead of the value of $3067.300224 \text{ cm}^{-1}$ reported by Abe *et al.* [57].

As indicated in Table 4, the speed dependence of the line broadening was set to $a_w = 0.110$ for fits F3 and F4. This value was obtained as follows. Figure 7 presents the values of a_w measured in fit F2 and the corresponding averages for each manifold. These averages do not exhibit any rotational dependence. They were therefore averaged, each value being multiplied by the inverse of the square of its standard deviation, yielding $a_w = 0.110(5)$. The results presented in Fig. 7 and their average are very similar to values reported in the literature, for example for methane [37, 65], carbon monoxide [66], carbon dioxide [67, 68] and acetylene [69].

Figures 3, 4 and 5 present the residuals obtained at the end of the fits performed in the present work for the P, Q and R branches, respectively. The sharp signatures observed for the lower pressures spectra (S2 and S3) are believed to arise from a still imperfect modeling of the ILS and a slight saturation of the stronger lines. The use of the relaxation matrix resulted in a clear reduction of the residuals for the more congested manifolds, *i.e.* R(9) to R(13) above 3110 cm^{-1} and, to a lesser extent, P(8) to P(11) below 2930 cm^{-1} . Shown in Fig. 6, the residuals obtained for the R(10) manifold are very revealing in that regard, where the first order approximation fails to represent the couplings involving the close lying lines of F symmetry observed between 3122.2 and 3122.5 cm^{-1} . However, no improvement in the residuals is observed for the more widespread lower J manifolds of the P and R branches, the signatures being even slightly larger in some cases [for R(6) and R(7), for example]. Figure 4 shows that the residuals exhibit a rather strong signature in the low J region of the Q branch. It is interpreted as resulting from the sum of many weak interactions that were neglected in the present modeling because of the above-mentioned restrictions, which had no consequence in the more widespread P and R branches. These restrictions made the general relaxation matrix equation manageable. In this case however, a hybrid method using both the relaxation matrix and first order line mixing should probably be used, as was done by Pine [37].

All the lines involving at least 1 fitted parameter in fits F1 and F4 are provided as supplementary material.

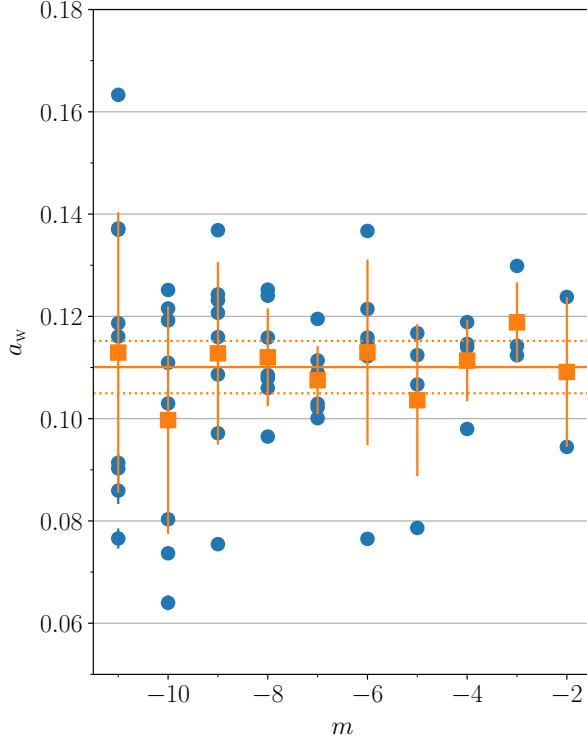


Figure 7: Speed dependence of line broadening coefficient a_w measured in the P branch of the ν_3 band of $^{12}\text{CH}_4$ in fit F2 ($m = -J''$). The blue circles are the measurements, the orange squares present the averages for each manifold (the error bars display the corresponding standard deviations) and the horizontal orange line shows the weighted average of the latter.

5. Results

The CO₂ broadening coefficients $b_L^0(\text{CO}_2)$, speed dependence of the broadening coefficient a_w , CO₂ shift coefficients δ^0 and first order line mixing parameters Y_n^0 measured in this work for the ν_3 band of $^{12}\text{CH}_4$ are presented in Figs. 8 and 11 to 13 ($m = -J''$, J'' and $J'' + 1$ for P, Q and R branch lines, respectively). As already highlighted, the 4 fits analyzed the P branch, fits F1 and F4 also dealt with the R branch and the Q branch was only studied in fit F4.

The uncertainties $\Delta\zeta$ on these measured parameters ζ , illustrated with error bars in the figures, were estimated using the following sum in quadrature

$$\Delta\zeta = \sqrt{(\delta\zeta)^2 + (\delta T)^2 + (\delta P_{tot})^2 + [\delta P(\text{CO}_2)]^2 + (\delta_{ils})^2} \quad (11)$$

In this expression, $\delta\zeta$ is the 1σ precision of measurement of the parameters, as provided by the least squares fitting algorithm. The uncertainty on the sample temperature was estimated to be $\delta T \approx 0.2\%$, from the sum in quadrature of the accuracy of measurement of the sensors (*i.e.* ± 0.3 K) and the uncertainty on the measured temperature itself (*i.e.* ± 0.5 K). The uncertainty on the measured total pressure is $\delta P_{tot} \approx 0.5\%$ (see Table 2). The uncertainties on the CO₂ pressures $\delta P(\text{CO}_2)$ include the uncertainties on the measured mole fractions of methane and the presence of impurities. They do not apply to the narrowing and line mixing parameters, involving the total pressure only (see Eqs. 7 and 8). The line shape exhibits similar behavior with respect to the Dicke

narrowing parameter and the speed dependence of broadening. The average covariance of the fit with respect to these two parameters, estimated to be equal to 10 % of their standard deviations, was therefore also considered for these two parameters. The contribution to the uncertainties on the measured parameters of uncertainties in the modeling of the instrument line shape (ILS) is identified by δ_{ils} in Eq. 11. It was estimated using a method similar to that described by Loos *et al.* [70]. A few manifolds were remeasured with the modulation function (from which the ILS is generated in the spectral domain) modified to minimize the sum of the square of the residuals obtained for each of them. The RMS of the differences between the values of the parameters obtained using the initial and modified ILS were used as the contributions δ_{ils} to their uncertainties. They amount to 0.4% for the broadening coefficients, 0.9% for the shift coefficients, 2.0% for the speed dependence of the broadening and 5.7% for the narrowing coefficients. As already observed [24, 70], the impact of uncertainties in the ILS was observed to be larger for smaller values of the line mixing parameters. δ_{ils} was therefore set to 3.4 and 3.2 % for $W_{mn} > 0.001 \text{ cm}^{-1}\text{atm}^{-1}$ and $Y_n^0 > 0.03 \text{ atm}^{-1}$, respectively. Smaller values of these 2 parameters were respectively assigned uncertainties $\delta_{ils} = 15$ and 18 %. Contrary to our previous contribution on the ν_3 band of methane [24], self broadening and self shift were considered in the present work. In that previous work, the neglect of self broadening was conservatively estimated to contribute 0.3 % to the uncertainties of the measured air broadening coefficients. Involving similar experimental conditions and noting that $b_L^0(\text{CO}_2) \simeq 1.2 \times b_L^0(\text{air})$ on average [12], the impact on $b_L^0(\text{CO}_2)$, a_w and β^0 of uncertainties on the self broadening coefficients listed in Table 3 was included in the present work. The value of $\delta^0(\text{self}) = -0.0090(13) \text{ cm}^{-1}\text{atm}^{-1}$ to which the self shift coefficients of all the methane lines were fixed to is similar to the CO₂ shift coefficients measured in this work (see Fig. 12). Even though Eq. 6 and the mole fractions listed in Table 2 show that the uncertainty of 14 % on $\delta^0(\text{self})$ contributes less than 0.2 % to the measured CO₂ shift coefficients, it was included in $\Delta\zeta$.

5.1. CO₂ broadening coefficients

The upper panel of Fig. 8 presents the CO₂ broadening coefficients measured in this work in the P, R and Q (fit F4 only) branches of the ν_3 band of ¹²CH₄ with line mixing modeled using the relaxation matrix formalism (fit F4) or the first order approximation (fit F1). Differences of the CO₂ broadening coefficients measured in fits F2, F3 and F4 with the values retrieved from fit F1 are presented in the lower 3 panels. Most of these differences are smaller than 1 % and their averages are $-0.22(1.4) \text{ \%}$, $-0.34(0.7) \text{ \%}$ and $0.18(1.6) \text{ \%}$ for fits F2, F3 and F4 ($m < 10$), respectively (the numbers between parentheses are the corresponding standard deviations). The largest difference of about 12 % is observed for the P(12, F_1 , 45, 1) line. The differences are somewhat larger for $m \geq 10$. The corresponding manifolds involve closely lying lines and the residuals obtained for these in fit F1 exhibit signatures (see Fig. 5) indicating that the first order line mixing model failed to reproduce satisfactorily the observed spectra. The resulting broadening coefficients retrieved from fit F1 may therefore be impacted by this imperfect modeling, leading to the large differences observed in the lower panel of Fig. 8.

Overall, the $b_L^0(\text{CO}_2)$ parameter is well decorrelated from the other parameters. The upper panel of Fig. 8 shows that the CO₂ broadening coefficients of lines of *E* symmetry tend to be smaller than for lines of *A* and *F* species, which do not exhibit any marked difference. This has been observed previously for different collision partners [24, 71–73] but the origin of such a behavior has not been clearly identified [74]. As is commonly observed for methane, all three branches exhibit the same J'' dependence, *i.e.* a decrease with increasing $|m|$ of the CO₂ broadening coefficients following a

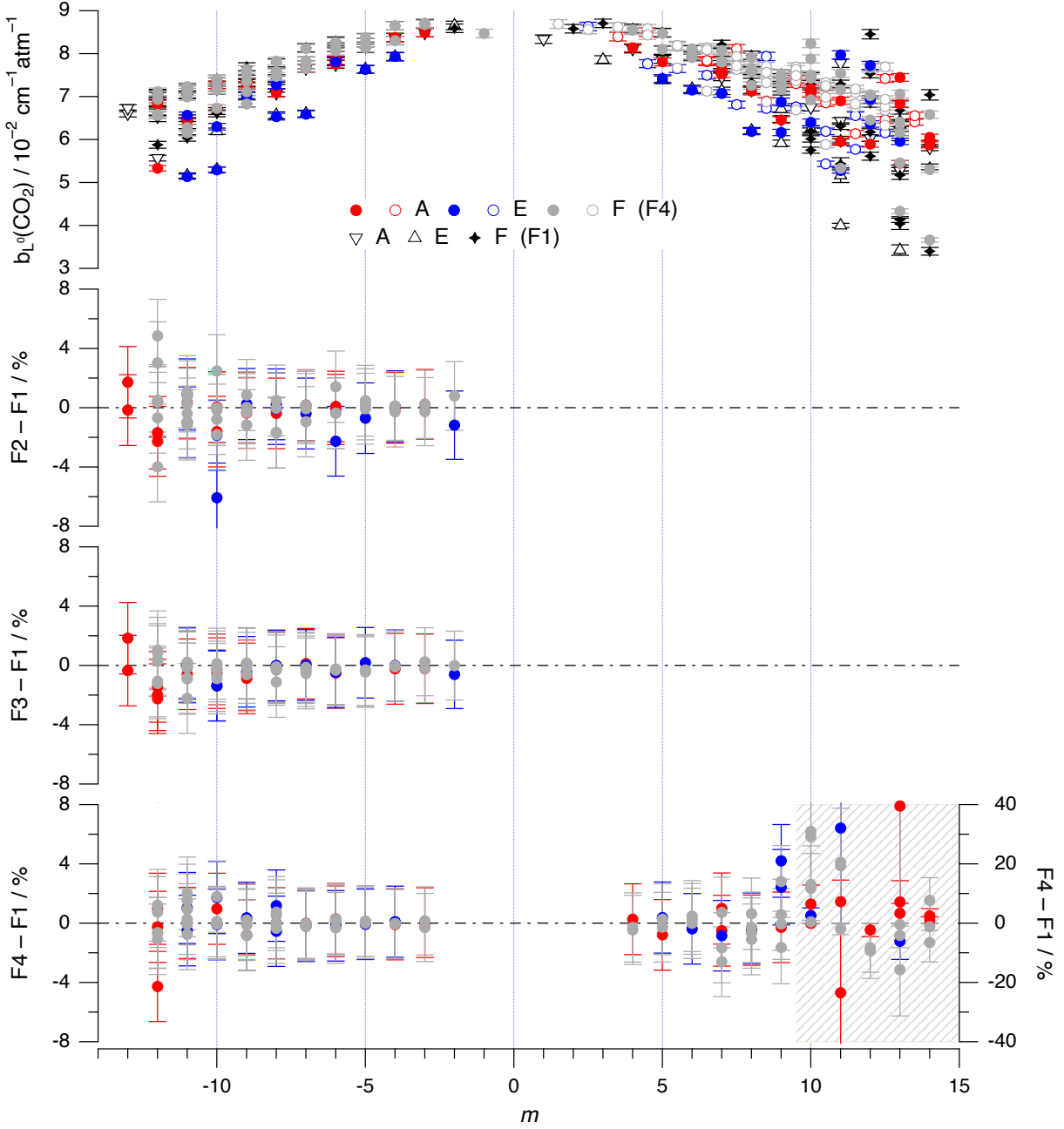


Figure 8: CO₂ broadening coefficient measured at 296.5 K in the P ($m = -J''$), Q ($m = J'' + 0.5$) and R ($m = J'' + 1$) branches of the ν_3 band of $^{12}\text{CH}_4$ with line mixing modeled using the relaxation matrix formalism (fit F4; colored symbols, filled for P and R branch lines and open for Q branch lines) and the first order approximation (fit F1, black symbols) (upper panel); differences with the CO₂ broadening coefficients measured in fit F1 of the values retrieved in fits F2, F3 and F4 are presented in the lower 3 panels. In the lower panel, the points over the hatched area refer to the right axis and three points, corresponding to differences of about 12 % at $m = -12$, 54 % at $m = 11$ and 71 % at $m = 13$, are off scale. The error bars represent the estimated uncertainties (see section 5 for details).

maximum near $|m| = 3$. This behavior has been attributed to the increase of the energy separation

between the rotational levels, leading to a reduction of the collisional transfer probabilities.

Table 5 and Fig. 9 compare the CO₂ broadening coefficients measured in this work with all the measurements reported for the ν_3 band of ¹²CH₄ [12, 16, 18]. As Es-sebbar and Farooq

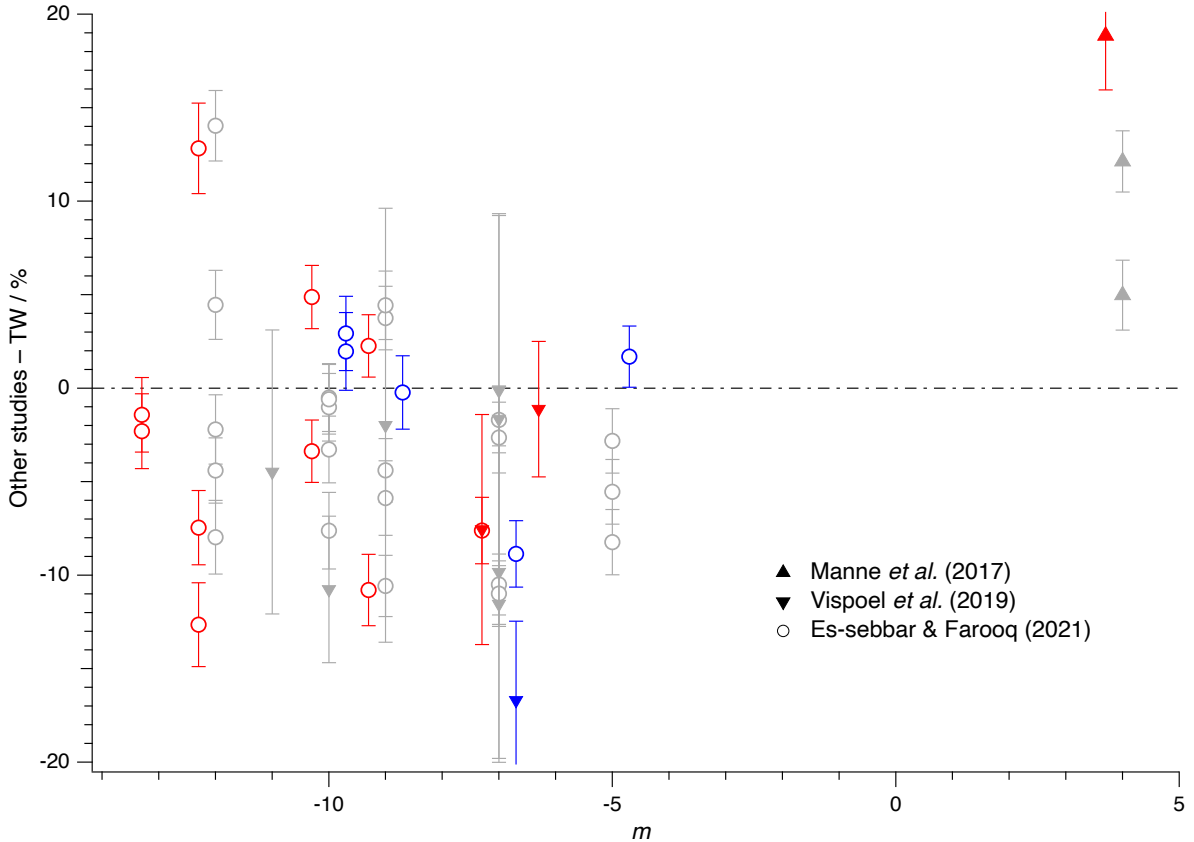


Figure 9: Differences with this work (TW) of CO₂ broadening coefficients for the ν_3 band of ¹²CH₄ measured in previous work (Manne *et al.* [18], Vispoel *et al.* [16] and Es-sebbar and Farooq [12]). Red, blue and grey symbols correspond to the *A*, *E* and *F* symmetries, respectively. To improve readability, the differences for the *A* and *E* symmetries are provided for $m - 0.3$ and $m + 0.3$, respectively.

[12] and Vispoel *et al.* [16] used several line shape models, the measurements performed using the profile closest to the one used in the present work were selected. Considering the uncertainties, the CO₂ broadening coefficients from Vispoel *et al.* [16] generally agree although some discrepancies are observed. They are however systematically lower than the present measurements. Those from Es-sebbar and Farooq [12] are closer to the present results although they also tend to be lower than the present results. This trend towards lower values of these two studies most probably results from the fact that the present analysis included both Dicke narrowing and speed dependence while these analyses only considered the former. The closer agreement of the present measurements with the results of Es-sebbar and Farooq [12] may originate from the fact that the use of the Galatry profile leads to broadening coefficients larger than the Rautian line shape model [16, 64]. The CO₂ broadening coefficients measured by Vispoel *et al.* [16] using the Galatry profile are indeed on average 2.6 % higher than measured using the Rautian profile. The measurements from Manne [18] show the opposite effect by not considering the Dicke narrowing.

Table 5: Comparison of CO₂ broadening coefficients (in 10⁻² cm⁻¹atm⁻¹) reported previously for the ν_3 band of ¹²CH₄ and measured in this work (TW). The numbers between parentheses are the uncertainties, given in the units of the last digits quoted.

J''	C''	α'	α''	[18] (qsdVoigt) [†]	[16] (Rautian)	[12] (Galatry)	TW
$P(13)$	A_2	18	1		6.456(53)	6.608(79)	
$P(13)$	A_1	16	1		6.636(54)	6.732(80)	
$P(12)$	A_1	15	2		5.968(71)	6.849(82)	
$P(12)$	F_1	43	3		7.514(45)	6.633(80)	
$P(12)$	F_2	45	3		7.245(45)	7.012(84)	
$P(12)$	A_2	14	1		6.425(55)	6.876(82)	
$P(12)$	F_2	46	2		6.547(55)	7.061(84)	
$P(12)$	F_1	44	2		6.729(39)	7.084(85)	
$P(12)$	F_2	47	1		6.428(43)	6.494(78)	
$P(12)$	A_1	16	1		6.016(65)	5.570(68)	
$P(11)$	F_1	42	2	6.840(459)		7.166(86)	
$P(10)$	F_2	37	3		7.118(45)	7.146(85)	
$P(10)$	E	24	2		5.449(42)	5.299(63)	
$P(10)$	F_1	36	2		7.164(44)	7.409(88)	
$P(10)$	A_1	14	1		7.025(34)	7.274(87)	
$P(10)$	F_1	37	1	6.560(200)	7.276(45)	7.351(88)	
$P(10)$	F_2	38	2		7.165(48)	7.212(86)	
$P(10)$	A_2	12	1		7.058(34)	6.665(80)	
$P(10)$	F_2	39	1		6.217(58)	6.611(79)	
$P(10)$	E	25	1		6.425(55)	6.194(75)	
$P(9)$	A_2	12	1		7.426(34)	7.320(87)	
$P(9)$	F_2	32	2		7.629(37)	7.411(88)	
$P(9)$	F_1	33	3		6.825(34)	7.696(92)	
$P(9)$	A_1	10	1		6.547(52)	7.321(87)	
$P(9)$	F_1	34	2		7.198(38)	7.513(90)	
$P(9)$	E	23	1		7.021(54)	7.012(84)	
$P(9)$	F_2	33	1	6.970(740)	7.426(45)	7.115(85)	
$P(9)$	F_1	35	1		6.428(54)	6.837(82)	
$P(7)$	F_1	26	2	6.980(679)	6.929(34)	7.744(92)	
$P(7)$	E	17	1	5.490(200)	6.006(38)	6.603(79)	
$P(7)$	F_2	24	2	7.180(590)	7.225(45)	8.136(97)	
$P(7)$	A_2	10	1	7.080(380)	7.076(45)	7.660(91)	
$P(7)$	F_2	25	1	7.820(640)	7.623(55)	7.835(93)	
$P(7)$	F_1	27	1	7.530(750)	7.526(44)	7.666(91)	
$P(6)$	A_2	6	1	7.760(190)		7.825(93)	
$P(5)$	F_1	18	2		7.685(44)	8.125(97)	
$P(5)$	E	12	1		7.763(34)	7.640(91)	
$P(5)$	F_2	17	1		8.142(44)	8.368(100)	
$P(5)$	F_1	19	1		7.578(45)	8.258(99)	
$R(3)$	A_2	7	1	9.670(139)		8.114(97)	
$R(3)$	F_2	15	1	8.970(60)		8.584(100)	
$R(3)$	F_1	16	1	9.600(40)		8.587(100)	

[†] “qsd” stands for “quadratic speed dependent.”

Figure 10 compares the present measurements for the ν_3 band with measurements reported for the ν_4 band [15] and 10 cold bands observed in the $5550 - 6140 \text{ cm}^{-1}$ range, involving changes of the vibrational quantum numbers up to 4 [14]. No obvious vibrational dependence can be put forward.

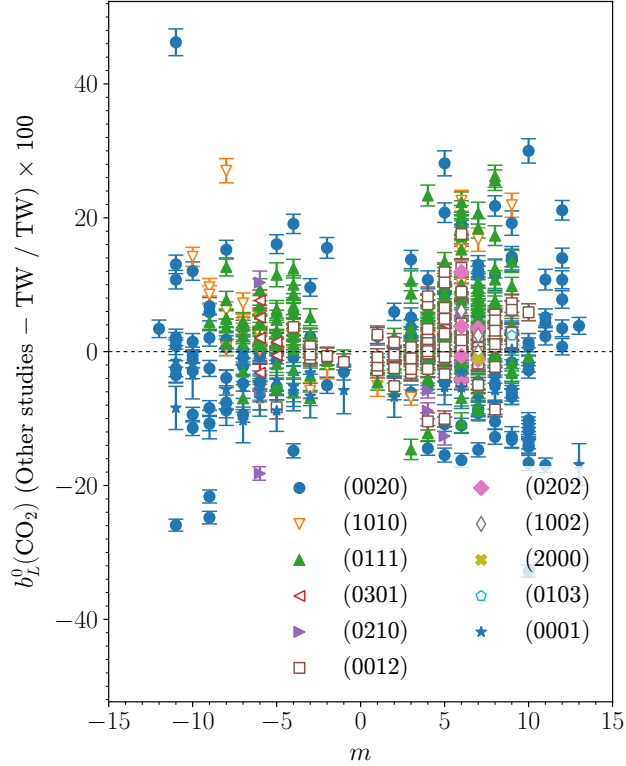


Figure 10: Differences with this work (TW) of CO₂ broadening coefficients reported for various cold bands of ¹²CH₄. The bands are identified with the upper vibrational level involved, *i.e.* ($v_1 v_2 v_3 v_4$) where v_i is the vibrational quantum number associated with the mode of vibration i . All the measurements are from Lyulin *et al.* [14], except for the ν_4 band [15].

5.2. Speed dependence of broadening

The speed dependence of line broadening coefficients a_w measured in this work in fits F1 and F4 are presented in the upper panel of Fig. 11, together with the average value $a_w = 0.110$ determined using a quadratic speed dependent Voigt profile to fit spectra at total pressures from 400 to 803 hPa (fit F2; see section 4). Differences of the a_w coefficients measured in fits F2 and F4 with the values retrieved from fit F1 are presented in the lower 2 panels. The averages of these differences are $-4.2(20.)\%$ and $1.3(21.)\%$ for fits F2 and F4 ($m < 10$), respectively. The differences presented in the lower panel of Fig. 11 are significantly larger for $m \geq 10$. These large differences may result from the imperfect modeling of the corresponding congested manifolds provided by the first order line mixing model (fit F1), as already discussed in section 5.1. However, the speed dependence coefficients measured in the Q branch in fit F4 exhibit a spread similar to the parameters retrieved in the R branch in fits F1 and F4 (see upper panel of Fig. 11) that may indicate that this spread has a physical origin.

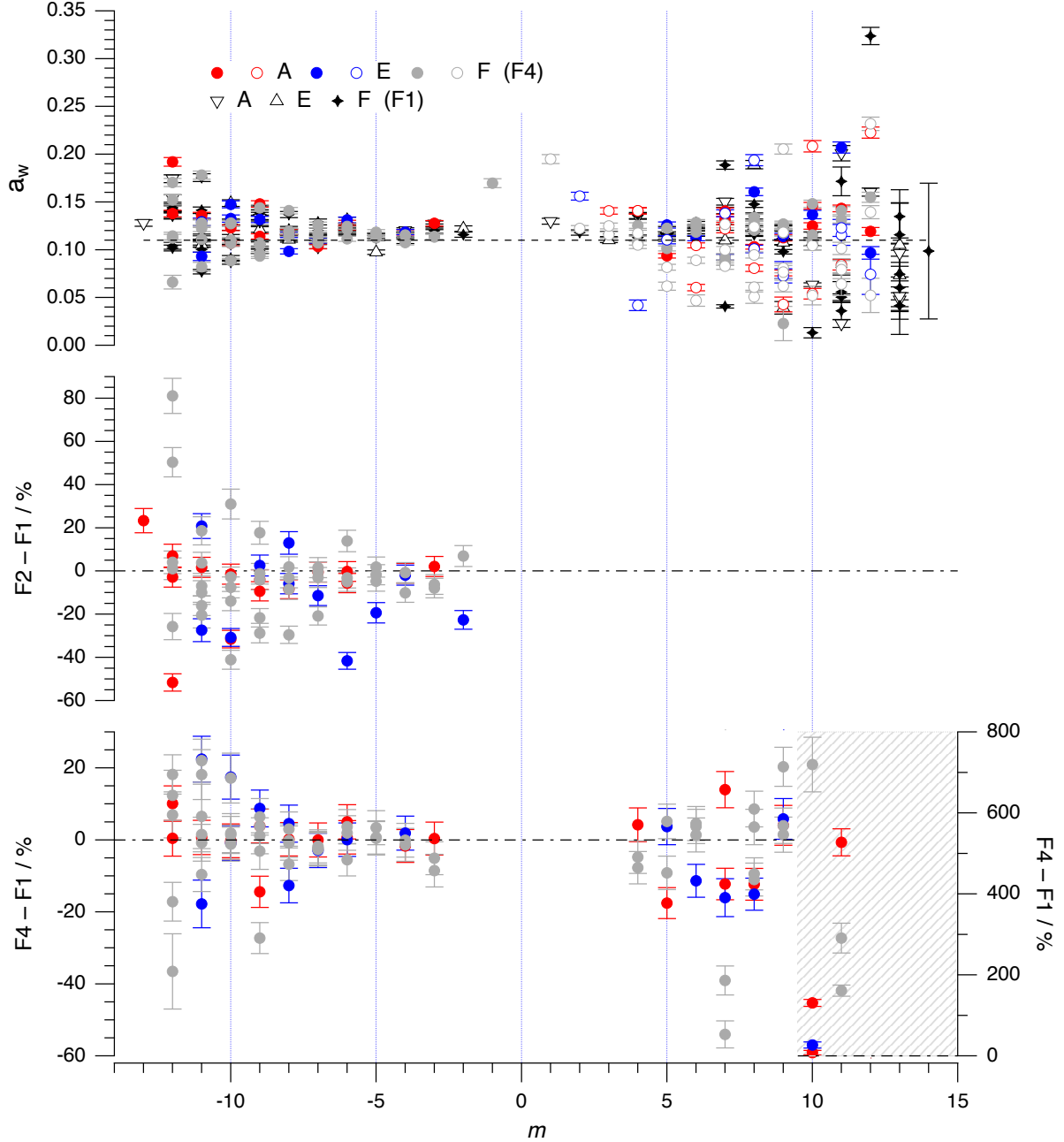


Figure 11: Speed-dependence of the broadening measured at 296.5 K in the P ($m = -J''$), Q ($m = J''$) and R ($m = J'' + 1$) branches of the ν_3 band of $^{12}\text{CH}_4$ with line mixing modeled using the relaxation matrix formalism (fit F4; colored symbols, filled for P and R branch lines and open for Q branch lines) and the first order approximation (fit F1, black symbols) (upper panel); differences with the speed dependence coefficients measured in fit F1 of the values retrieved in fits F2 and F4 are presented in the lower 2 panels. In the lower panel, the points over the hatched area refer to the right axis. The error bars represent the estimated uncertainties (see section 5 for details).

Although the a_w coefficients presented in the upper panel of Fig. 11 seem to be on average larger in the P branch than in the R and Q branches, the spread of the data prevents any definite

conclusion on a possible rotational dependence to be drawn. Additionally, the data do not exhibit any obvious dependence on the tetrahedral symmetry, unlike the broadening coefficients. As already indicated, the range of a_w values obtained in this work is similar to what is reported in the literature for methane and other molecules [37, 65–69]. The few values measured for $|m| \leq 2$ in the Q branch are high compared to neighboring data. This is likely due to the combined effects of the lower intensity of the corresponding lines and correlations between speed dependence, narrowing and residual line mixing.

The a_w coefficients determined in fit F2 [from which the average value $a_w = 0.110(5)$ was determined] are on average 4 – 5 % smaller than in the other 2 fits, as highlighted by the negative average differences mentioned here above. This may indicate that narrowing was underestimated in fits F1 and F4 and speed dependence consequently overestimated, implying that the two parameters are still correlated with the range of pressures used in the present work. This point is further discussed in section 5.3.

Table 6 compares the speed dependence of broadening coefficients a_w measured in fits F1 and F4 with values reported by Manne *et al.* [18], retrieved using a quadratic speed dependent Voigt profile with first order line mixing. The latter are about an order of magnitude smaller than determined in the present work. The origin of this discrepancy is unclear. It may come from the different ranges

Table 6: Speed dependence of the broadening a_w (unitless) for the R(3) manifold of the ν_3 band of $^{12}\text{CH}_4$ measured in fits F1 and F4 of this work (TW) and reported by Manne *et al.* [18]. The numbers between parentheses are the uncertainties, given in the units of the last digits quoted.

	C''	α'	α''	[18]	TW (F4)	TW (F1)
A_2	7	1	0.012 (7)	0.1407 (32)	0.1350 (31)	
F_2	15	1	0.008 (7)	0.1253 (29)	0.1358 (32)	
F_1	16	1	0.01 (3)	0.1074 (25)	0.1128 (26)	

of total pressures used in the two studies, *i.e.* up to 803 hPa in the present work and up to 200 hPa in [18]. The rather large uncertainties characterizing the values reported in [18] possibly indicate that the range of total pressures was too low.

5.3. Dicke narrowing

The Dicke narrowing coefficients β^0 were measured for several lines of the P and R branches of the ν_3 band of $^{12}\text{CH}_4$ in fits F1 and F3, and for the 3 branches in fit F4. They seemed to exhibit a rotational dependence, whereas β^0 is expected to be constant for the uncorrelated hard collision line shape model [51] because collisional broadening and the Doppler effect can be considered as statistically independent. Although it may only be apparent, resulting from the increasing dispersion of the measured values that follows the increasing number of lines per manifold as J becomes larger, the observation of such a rotational dependence was interpreted as resulting from the correlation between the measured Dicke narrowing coefficients and speed dependence of broadening, even though their contributions to the observed spectra dominate in different pressure regimes (*i.e.* intermediate pressures for the former and higher pressures for the latter). Fit F3 provided another indication of the existence of such a correlation. Indeed, it involved decorrelating β^0 and a_w by fixing the latter. The spread of the measured narrowing coefficients was found to be similar to fits F1 and F4, but any resemblance of a J'' dependence was absent.

The rough average of the Dicke narrowing coefficients measured in the present work is $\langle \beta^0 \rangle \approx 0.005 \text{ cm}^{-1}\text{atm}^{-1}$. To the best of our knowledge, narrowing coefficients were only reported twice for the ν_3 band of methane perturbed by CO₂, from measurements carried out using the Galatry profile in spectra recorded at 297(1) K. Performed in the P(11) manifold observed at total pressures up to 101 torr, these measurements yielded an average narrowing coefficient of $\langle \beta^0 \rangle = 0.02724(43) \text{ cm}^{-1}\text{atm}^{-1}$ [17]. A more precise average of $\langle \beta^0 \rangle = 0.02934(18) \text{ cm}^{-1}\text{atm}^{-1}$ was recently reported by the same authors, from a more extensive study of the P branch relying on spectra recorded at total pressures between 4 and 201 torr [12].

The rather small Dicke narrowing coefficients obtained in the present work together with the possible correlation with speed dependence were interpreted as an indication that the present measurements did not rely on enough spectra corresponding to total pressures below about 200 hPa. Indeed, Fig. 2 shows that Dicke narrowing effects are largest in that range of pressures. Hence, the narrowing coefficients measured in the present work should probably be considered as fitting parameters only and their values are therefore not reported.

5.4. CO₂ shift coefficients

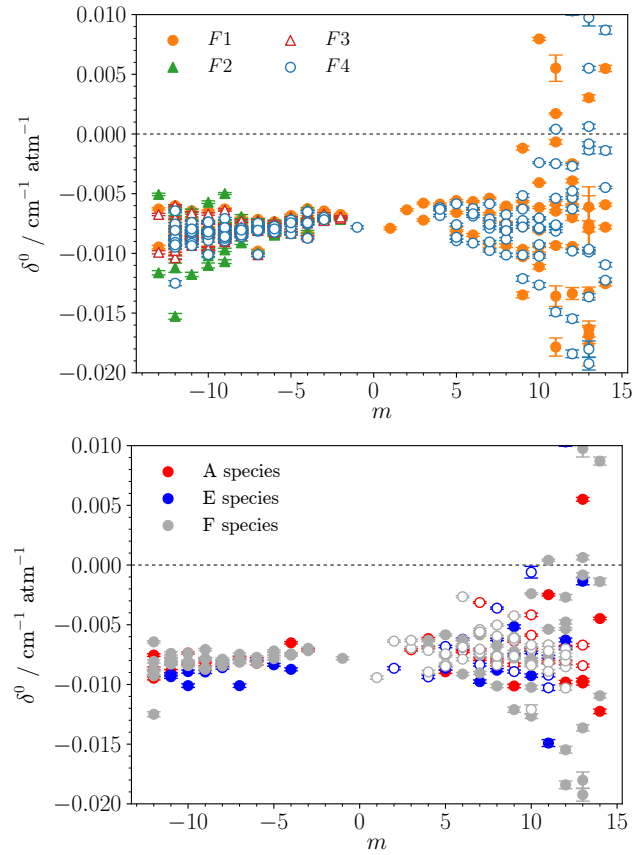


Figure 12: CO₂ shift coefficients measured at 296.5 K in the P ($m = -J''$) and R ($m = J'' + 1$) branches of the ν_3 band of ¹²CH₄ through the 4 fits described in Table 4 (upper panel) and results obtained using the relaxation matrix formalism (fit F4) for the P, Q ($m = J''$, open symbols) and R branches (lower panel).

The CO₂ shift coefficients measured in fits F1 to F4 are presented in the upper panel of Fig.

12. To the best of our knowledge, this is the first time that these coefficients are measured for the ν_3 band of methane. The spread of the reported shift parameters is larger in the R branch, particularly for $m \geq 10$. As already noted for the speed dependence coefficients and because it is observed for fits F1 and F4, it is unclear whether this trend is real or results from some imperfect modeling of line mixing in the corresponding congested manifolds.

The absolute value of the shift coefficients resulting from fit F1 clearly appear to be systematically smaller than those obtained from the other 3 fits, by about 4 – 5 %. The origin of this difference is unclear. It could come from correlations between the CO₂ shift and first order line mixing coefficients, but none was observed. Figure 12 also shows that the more limited range of pressures characterizing fit F2 had visible consequences on the precision of measurement of the shift coefficients. This observation highlights the sensitivity of this parameter to the experimental information available.

The CO₂ shift coefficients resulting from fit F4 with distinction between A, E and F species are presented in the lower panel of Fig. 12. In the P branch, the lines of E symmetry seem to undergo more shift than the other lines. This possible trend is however not visible in the other branches, preventing any definite conclusion to be drawn.

5.5. First order line mixing model

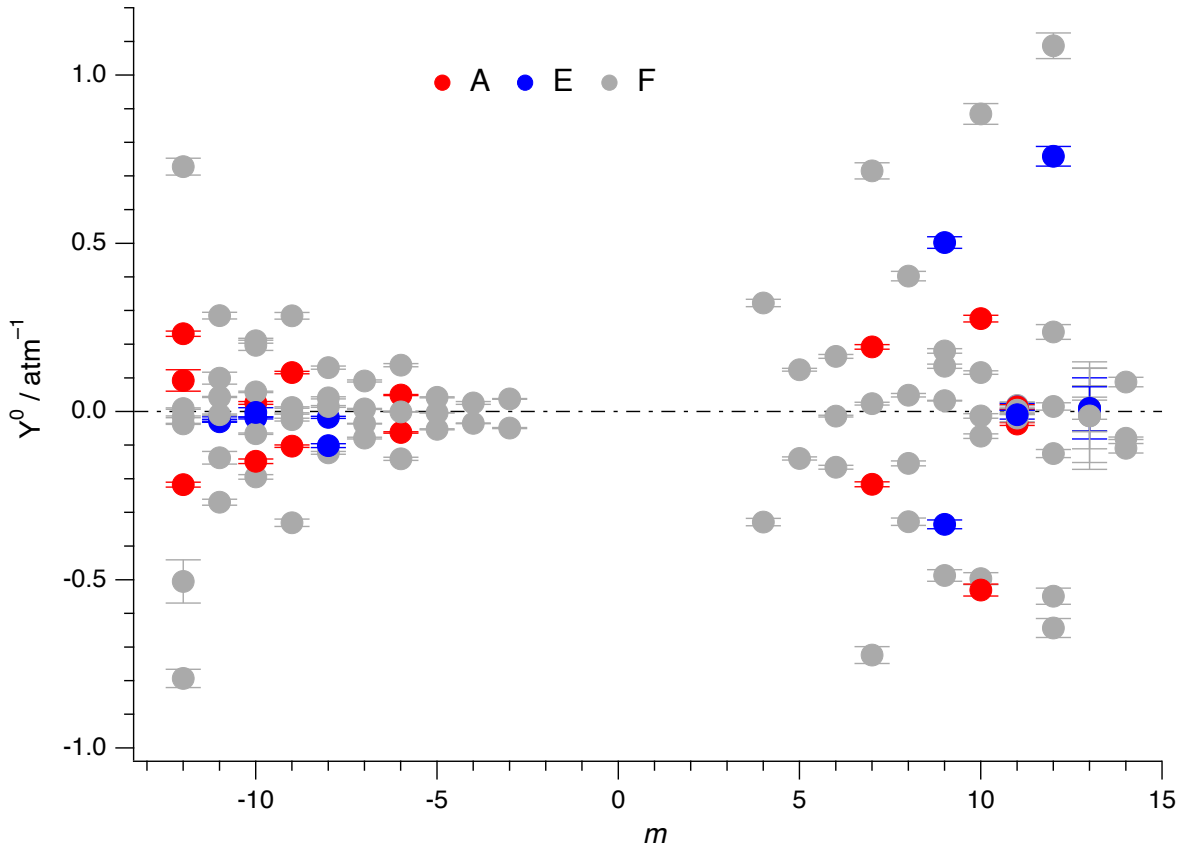


Figure 13: First order line mixing coefficients measured at 296.5 K in the P ($m = -J''$) and R ($m = J'' + 1$) branches of the ν_3 band of $^{12}\text{CH}_4$ in fit F1.

Table 7 lists the first order line mixing coefficients Y_n^0 measured in fit F1 for 111 lines of the ν_3 band of $^{12}\text{CH}_4$. They are presented in Fig. 13. Table 7 includes two additional Y_n^0 values, associated with lines of the $\nu_2 + \nu_4$ (F_2) band and also fitted to improve the residuals. The Y_n^0 coefficients of all the other lines were set to zero. Fits F2 and F3 yield very similar results for the P branch and are therefore not presented. As also observed for the ν_3 band of $^{12}\text{CH}_4$ perturbed by air [24], most line mixing coefficients are in the range from -0.5 to 0.5 atm^{-1} .

Table 7: First order line mixing coefficients $Y_n^0(\text{F1})$ and $Y_n^0(\text{F4})$ (in atm^{-1}) for the ν_3 band of $^{12}\text{CH}_4$ measured in fit F1 and calculated using Eq. 10, respectively. The number provided between parentheses after each value is the estimated uncertainty, in the units of the last digit quoted. Its absence for $Y_n^0(\text{F4})$ indicates that it is larger than 0.1 or the value of $Y_n^0(\text{F4})$. The identification, position $\tilde{\nu}_n$ (in cm^{-1}) and intensity I_n [in $10^{-21} \text{ cm}^{-1}/(\text{molecule cm}^{-2})$] of the lines are from the HITRAN database [22]. Two lines (identified by \dagger) belong to the $\nu_2 + \nu_4$ (F_2) band. In the column labeled “ W_{mn} ,” the first (*resp.* second) pair of digits $i:j$ refers to the $A_1 \leftrightarrow A_2$, $E \leftrightarrow E$ and $F_1 \leftrightarrow F_2$ [*resp.* $(A \text{ or } F)_1 \leftrightarrow (A \text{ or } F)_1$ and $(A \text{ or } F)_2 \leftrightarrow (A \text{ or } F)_2$] couplings: i is the number of couplings considered in fit F4 and j is the total number of possible couplings involving line n in the J'' manifold it belongs to.

Line n	$\tilde{\nu}_n$	I_n	$Y_n^0(\text{F1})$	$Y_n^0(\text{F4})$	W_{mn}
P(12, A_1 , 2, 15)	2894.9961	11.09	0.2314 (79)	0.2123 (78)	1:1/0:1
P(12, F_1 , 3, 43)	2895.0560	6.618	0.7277 (250)	0.6446 (238)	1:3/0:2
P(12, F_2 , 3, 45)	2895.1288	6.561	-0.7930 (270)	-0.6502 (240)	1:3/0:2
P(12, A_2 , 1, 14)	2895.2333	11.02	-0.2172 (74)	-0.2138 (79)	1:2/0:0
P(12, F_2 , 2, 46)	2895.7573	6.439	0.0089 (20)		
P(12, F_1 , 2, 44)	2896.2026	6.521	-0.0367 (15)		
P(12, F_2 , 1, 47)	2896.2999	6.523	-0.0158 (28)		
P(12, F_1 , 1, 45)	2896.9801	6.696	-0.5051 (640)		
P(12, A_1 , 1, 16)	2896.9902	11.16	0.0922 (320)		
P(11, F_1 , 3, 41)	2905.6337	11.32	0.2852 (97)	0.2626	3:3/2:2
P(11, E , 2, 27)	2905.6975	7.486	-0.0191 (34)		
P(11, F_2 , 3, 39)	2905.8137	11.40	-0.2694 (91)	-0.2514	3:3/2:2
P(11, F_1 , 2, 42)	2906.2825	11.06	0.0435 (15)	0.0459	3:3/2:2
P(11, E , 1, 28)	2906.5888	7.389	-0.0303 (18)		
P(11, F_2 , 2, 40)	2906.6476	11.10	-0.0093 (19)	-0.0230	3:3/2:2
P(11, F_2 , 1, 41)	2907.3213	11.41	-0.1372 (190)	0.0271	3:3/2:2
P(11, F_1 , 1, 43)	2907.3361	11.41	0.0991 (180)	-0.0587	3:3/2:2
P(10, F_2 , 3, 37)	2916.2016	18.36	0.2107 (72)	0.1972 (73)	1:2/0:2
P(10, E , 2, 24)	2916.3018	12.07	-0.0190 (33)		
P(10, F_1 , 2, 36)	2916.3963	17.87	-0.1944 (66)	-0.1914 (79)	3:3/0:1
P(10, A_1 , 1, 14)	2916.7538	29.62	0.0257 (44)	0.0269 (10)	1:1/0:0
P(10, F_1 , 1, 37)	2916.9662	17.70	0.0584 (20)	0.0595 (23)	3:3/0:1
P(10, F_2 , 2, 38)	2917.0661	17.88	-0.0659 (23)	-0.0643 (24)	1:2/1:2
P(10, A_2 , 1, 12)	2917.6291	30.55	-0.1477 (69)	-0.0261 (10)	1:1/0:0
P(10, F_2 , 1, 39)	2917.6526	18.31	0.1971 (150)	-0.0057 (3)	1:2/0:2
P(10, E , 1, 25)	2917.6628	12.22	-0.0027 (140)		
P(9, A_2 , 1, 12)	2926.7002	45.83	0.1161 (39)	0.1020 (38)	1:1/0:0
P(9, F_2 , 2, 32)	2926.7830	27.36	0.2844 (97)	0.2954 (109)	2:3/0:1
P(9, F_1 , 3, 33)	2926.8851	27.09	-0.3304 (110)	-0.2984 (110)	1:2/0:2
P(9, A_1 , 1, 10)	2927.0762	45.46	-0.1029 (35)	-0.1029 (38)	1:1/0:0
P(9, F_1 , 2, 34)	2927.3726	26.82	0.0123 (21)	0.0196 (7)	1:2/1:2
P(9, F_2 , 1, 33)	2927.9321	27.65	-0.0060 (20)	-0.0028	2:3/0:1

Continued on next page

Table 7: (Continued)

Line n	$\tilde{\nu}_n$	I_n	$Y_n^0(\text{F1})$	$Y_n^0(\text{F4})$	W_{mn}
P(9, F_1 , 1, 35)	2927.9636	27.65	-0.0240 (44)	-0.0163 (31)	1:2/0:2
P(8, F_2 , 2, 30)	2937.2346	38.80	0.1307 (45)	0.1215 (45)	2:2/0:1
P(8, E , 2, 19)	2937.3082	25.71	-0.0173 (30)	0.0005	1:1/0:0
P(8, F_1 , 2, 28)	2937.4950	38.53	-0.1229 (42)	-0.1173 (54)	2:2/0:1
P(8, F_2 , 1, 31)	2937.7672	38.17	0.0154 (26)	0.0179 (18)	2:2/1:1
P(8, E , 1, 20)	2938.1926	26.06	-0.1015 (55)	-0.0005	1:1/0:0
P(8, F_1 , 1, 29)	2938.2154	39.10	0.0407 (32)	-0.0225 (9)	1:2/0:1
P(7, F_1 , 2, 26)	2947.6680	51.28	0.0908 (31)	0.0938 (52)	2:2/1:1
P(7, F_2 , 2, 24)	2947.9121	50.69	-0.0787 (27)	-0.0711 (150)	2:2/1:1
P(7, F_2 , 1, 25)	2948.4214	51.49	0.0079 (14)	0.0111	2:2/1:1
P(7, F_1 , 1, 27)	2948.4741	51.71	-0.0359 (13)	-0.0344 (131)	2:2/1:1
P(6, A_1 , 1, 8)	2958.0173	105.2	0.0488 (17)	0.0545 (20)	1:1/0:0
P(6, F_1 , 1, 21)	2958.1200	62.73	0.1378 (47)	0.1355 (49)	1:2/0:0
P(6, F_2 , 2, 22)	2958.2329	62.26	-0.1407 (48)	-0.1337 (54)	1:1/1:1
P(6, A_2 , 1, 6)	2958.5364	105.7	-0.0623 (21)	-0.0543 (20)	1:1/0:0
P(6, F_2 , 1, 23)	2958.6508	63.15	-0.0009 (3)	-0.0027 (4)	1:1/0:1
P(5, F_1 , 2, 18)	2968.4033	70.85	0.0423 (14)	0.0495 (18)	1:1/0:1
P(5, F_2 , 1, 17)	2968.7362	71.41	-0.0530 (18)	-0.0469 (22)	2:2/0:0
P(5, F_1 , 1, 19)	2968.8552	71.30	-0.0035 (6)	-0.0022 (4)	1:1/0:1
R(7, F_2 , 1, 25)	2971.0753	1.956	0.0257 (47)		
R(7, F_1 , 1, 26)	2971.2826	1.995	-0.0824 (33)		
P(4, F_2 , 1, 15)	2978.6505	72.12	0.0256 (44)	0.0271 (10)	1:1/0:0
P(4, F_1 , 1, 13)	2978.9199	72.54	-0.0351 (12)	-0.0270 (10)	1:1/0:0
P(3, F_2 , 1, 9)	2988.9325	64.33	0.0375 (13)	0.0524 (19)	1:1/0:0
P(3, F_1 , 1, 11)	2989.0335	64.53	-0.0493 (17)	-0.0522 (19)	1:1/0:0
R(3, F_2 , 1, 15)	3057.7265	126.0	0.3227 (110)	0.3250 (123)	1:1/0:0
R(3, F_1 , 1, 16)	3057.7607	126.0	-0.3284 (110)	-0.3250 (123)	1:1/0:0
R(4, F_2 , 1, 20)	3067.1642	127.4	0.1242 (42)	0.1127 (41)	1:1/0:0
R(4, F_1 , 1, 18)	3067.2611	126.6	-0.1392 (47)	-0.1135 (41)	1:1/0:0
R(5, F_1 , 2, 23)	3076.5496	117.9	0.1638 (56)	0.1627 (59)	2:2/0:1
R(5, F_2 , 1, 21)	3076.6770	116.6	-0.1656 (56)	-0.1529 (78)	2:2/0:1
R(5, F_1 , 1, 24)	3076.7252	117.0	-0.0138 (24)	-0.0116 (18)	2:2/0:1
R(6, A_1 , 1, 10)	3085.8322	169.3	0.1922 (66)	0.1712 (63)	1:2/0:0
R(6, F_1 , 1, 25)	3085.8607	101.3	0.7153 (240)	0.6799 (251)	2:3/0:0
R(6, F_2 , 2, 26)	3085.8935	101.1	-0.7238 (250)	-0.6518 (238)	1:1/1:2
R(6, A_2 , 1, 8)	3086.0308	165.9	-0.2162 (74)	-0.1747 (64)	1:1/0:1
R(6, F_2 , 1, 27)	3086.0717	100.0	0.0234 (41)	-0.0298 (14)	1:1/1:2
R(7, F_1 , 2, 29)	3095.0607	81.50	0.4024 (140)	0.3673 (147)	2:3/0:2
R(7, F_2 , 2, 28)	3095.1307	80.95	-0.3273 (110)	-0.2724 (134)	2:3/0:2
R(7, F_2 , 1, 29)	3095.3511	79.61	0.0488 (51)	0.0377 (120)	2:3/0:2
R(7, F_1 , 1, 30)	3095.3710	79.83	-0.1543 (71)	-0.1365 (106)	2:3/0:2
R(8, F_2 , 2, 33)	3104.2054	61.33	0.1801 (66)	0.4570 (172)	3:3/0:1
R(8, E , 2, 21)	3104.2206	40.81	0.5026 (170)	0.0535 (38)	1:2/0:0
R(8, F_1 , 2, 31)	3104.2840	60.75	-0.4873 (170)	-0.4056 (246)	2:2/1:2
R(8, F_2 , 1, 34)	3104.3365	60.81	0.0323 (13)	-0.0012	3:3/0:1
R(8, E , 1, 22)	3104.5690	39.67	-0.3352 (130)	-0.0551 (40)	1:2/0:0
R(8, F_1 , 1, 32)	3104.5749	59.56	0.1345 (61)	-0.0557 (75)	2:2/1:2

Continued on next page

Table 7: (Continued)

Line n	$\tilde{\nu}_n$	I_n	$Y_n^0(\text{F1})$	$Y_n^0(\text{F4})$	W_{mn}
R(9, A_2 , 1, 13)	3113.2615	72.54	0.2761 (100)	0.3680 (135)	1:2/0:0
R(9, F_2 , 2, 34)	3113.2798	43.35	-0.4968 (180)	1.826 (757)	2:6/0:2
R(9, F_1 , 3, 36)	3113.3012	41.72	0.8844 (310)	-1.757 (779)	1:3/1:5
R(9, A_1 , 1, 12)	3113.3803	71.52	-0.5304 (180)	-0.3733 (137)	1:1/0:1
R(9, F_1 , 2, 37)	3113.4174	41.33	0.1158 (54)	-0.0653 (261)	1:3/2:5
R(9, F_2 , 1, 35)	3113.7073	41.82	-0.0133 (66)	3.758	2:6/0:2
R(9, F_1 , 1, 38)	3113.7119	41.80	-0.0730 (66)	-3.836	1:3/0:5
R(10, F_2 , 3, 39)	3122.2575	28.65	0.0183 (84)	0.8407 (317)	2:4/0:3
R(10, E , 2, 26)	3122.2853	19.13	0.0140 (100)		
R(10, F_1 , 2, 38)	3122.2962	23.98	0.0137 (150)	-0.6307 (297)	1:4/1:3
R(10, A_1 , 1, 14)	3122.3316	48.37	0.0135 (69)	0.0447 (28)	1:2/0:0
R(10, F_1 , 1, 39)	3122.4393	23.62	0.0044 (130)	13.3	1:4/2:3
R(10, F_2 , 2, 40)	3122.4440	28.16	0.0027 (77)	-11.3	2:4/0:3
R(10, A_2 , 1, 12)	3122.7625	46.27	-0.0371 (40)	-0.0471 (30)	1:1/0:1
R(10, E , 1, 27)	3122.7647	18.36	-0.0096 (130)		
R(10, F_2 , 1, 41)	3122.7639	27.57	-0.0194 (110)	-0.1704 (68)	1:4/0:3
R(11, E , 2, 28)	3131.1704	9.139	0.7590 (290)		
R(11, F_1 , 3, 43)	3131.1737	17.12	1.0870 (380)	1.310 (507)	2:5/0:2
R(11, F_2 , 3, 41)	3131.2065	10.46	-0.6434 (280)	-1.395 (811)	2:3/0:4
R(11, F_1 , 2, 42)	3131.2426	17.37	-0.5490 (240)	-0.4394 (236)	2:5/0:2
R(11, F_2 , 2, 41)	3131.3472	7.526	0.2366 (220)		
R(11, F_2 , 1, 43)	3131.7352	17.25	0.0152 (110)	85.6	1:3/0:4
R(11, F_1 , 1, 44)	3131.7362	16.97	-0.1249 (120)	-87.1	2:5/0:2
R(12, F_1 , 3, 45)	3140.0447	6.262	0.0099 (670)	3.336	2:6/0:4
R(12, F_2 , 3, 48)	3140.0660	8.062	0.0098 (330)	15.3	2:5/0:5
R(12, F_2 , 2, 46)	3140.0686	9.040	0.0095 (1200)	-16.0	2:5/0:5
R(12, E , 2, 30)	3140.0836	7.090	0.0095 (910)		
R(12, F_1 , 2, 44)	3140.2204	6.394	-0.0123 (1600)		
R(12, F_2 , 1, 47)	3140.2230	7.250	-0.0116 (1400)		
R(12, E , 1, 31)	3140.6222	6.764	0.0080 (660)		
R(12, F_1 , 1, 46)	3140.6256	9.661	-0.0132 (470)		
R(13, F_2 , 2, 47)	3148.8237	5.224	0.0877 (140)		
R(13, F_2 , 3, 49)	3148.8299	5.522	-0.1091 (140)		
R(13, F_2 , 1, 48)	3149.4217	5.222	-0.0793 (37)		

Since the elements of the relaxation matrix verify the detailed balance relation ensuring that the total population is conserved, the first order line mixing coefficients Y_n^0 must satisfy the following sum rule [34]:

$$\sum_n \rho_n(T) \mu_n^2 Y_n^0 = 0 \quad (12)$$

where T is the temperature, ρ_n is the relative population of the lower level of the transition corresponding to line n (see Eq. 3) and the sum runs over all the lines of a given symmetry in a given P, Q or R manifold. As the relative populations ρ_n are approximately the same for all transitions in the same multiplet, the average of the coefficients measured for given m and symmetry is close to zero. The first order line mixing coefficients associated with close lying doublets of lines even appear in pairs of similar absolute values and opposite signs, as can be clearly seen in Fig. 13

for lines of F symmetry.

In the P branch, large line mixing coefficients were obtained for high J lines. Most probably, these result from the combined effects of the increasing density of lines in the corresponding multiplets and the decreasing intensity of these lines. The spread of the line mixing coefficients is significantly larger in the R branch as a result of its more coupled nature, leading to the failure of the first order line mixing model as observed in Figs. 5 and 6. Interestingly, the axial symmetry of the coefficients starts to break where signatures in the residuals start to appear (at $m = 10$ in Fig. 5).

Table 8 compares the first order line mixing coefficients measured in the present work with the only data reported in the literature [18]. As the couplings are weak in the R(3) manifold, the first order approximation works very well and leads to good agreement. Contrary to the present work, Manne *et al.* [18] did consider the 10 times smaller line mixing for the A_2 line but this had little impact.

Table 8: First order line mixing coefficients Y_n^0 (atm^{-1}) for the R(3) manifold of the ν_3 band of $^{12}\text{CH}_4$ measured in fit F1 of this work (TW) and reported by Manne *et al.* [18]. The numbers between parentheses are the uncertainties, given in the units of the last digits quoted.

	C''	α'	α''	[18]	TW
A_2	7	1	0.03 (12)	0.0 (fixed)	
F_2	15	1	0.39 (9)	0.323 (11)	
F_1	16	1	-0.35 (12)	-0.328 (11)	

5.6. Relaxation matrix formalism

Involving lines of the ν_3 band of $^{12}\text{CH}_4$, the 114 off-diagonal relaxation matrix coefficients measured in this work are listed in Table 9. 109 coefficients couple lines stronger than $10^{-20} \text{ cm}^{-1}/(\text{molecule cm}^{-2})$. The 5 remaining parameters were considered as they improved the residuals. They involved 7 close-lying ($|\Delta\tilde{\nu}| \leq 0.1 \text{ cm}^{-1}$) weaker ($6.6 \times 10^{-21} < \text{intensity} < 9.0 \times 10^{-21}$) lines of the P, Q and R branches with $J'' = 12$.

Table 9: Off-diagonal relaxation matrix coefficients W_{mn} (in $10^{-2} \text{ cm}^{-1}\text{atm}^{-1}$) measured in this work (column “TW”) for the ν_3 band of $^{12}\text{CH}_4$. The estimated uncertainty is provided between parentheses after each value, in the units of the last digit quoted. Zero indicates that the measured value was smaller than its estimated uncertainty. Off-diagonal coefficients not listed were fixed to zero. Column “Lit.” lists the values calculated for $\text{CH}_4\text{-air}$ in [75], multiplied by 1.3 (as done in [11]). The identifications of the lines are from the HITRAN database [22].

Line m	Line n	TW	Lit.	Line m	Line n	TW	Lit.
P(12, A_1 , 2, 15)	P(12, A_2 , 1, 14)	2.527 (93)	3.151	R(3, F_2 , 1, 15)	R(3, F_1 , 1, 16)	0.556 (21)	0.449
P(12, F_1 , 3, 43)	P(12, F_2 , 3, 45)	2.358 (87)	2.680	R(4, F_2 , 1, 20)	R(4, F_1 , 1, 18)	0.548 (20)	0.380
P(11, F_1 , 3, 41)	P(11, F_2 , 3, 39)	2.350 (100)	3.259	R(5, F_1 , 2, 23)	R(5, F_2 , 1, 21)	1.042 (38)	1.529
P(11, F_1 , 3, 41)	P(11, F_1 , 2, 42)	0.0	0.002	R(5, F_1 , 2, 23)	R(5, F_1 , 1, 24)	0.0	0.020
P(11, F_1 , 3, 41)	P(11, F_2 , 2, 40)	0.0	0.329	R(5, F_2 , 1, 21)	R(5, F_1 , 1, 24)	0.028 (4)	0.082
P(11, F_1 , 3, 41)	P(11, F_2 , 1, 41)	0.0	0.008	R(6, F_1 , 1, 25)	R(6, F_2 , 2, 26)	1.070 (39)	1.254
P(11, F_1 , 3, 41)	P(11, F_1 , 1, 43)	0.0	0.047	R(6, F_1 , 1, 25)	R(6, F_2 , 1, 27)	0.312 (15)	0.474
P(11, F_2 , 3, 39)	P(11, F_1 , 2, 42)	0.0	0.064	R(6, F_2 , 2, 26)	R(6, F_2 , 1, 27)	0.0	0.070
P(11, F_2 , 3, 39)	P(11, F_2 , 2, 40)	0.0	0.039	R(6, A_1 , 1, 10)	R(6, A_2 , 1, 8)	1.717 (63)	2.010
P(11, F_2 , 3, 39)	P(11, F_2 , 1, 41)	0.0	0.006	R(7, F_1 , 2, 29)	R(7, F_2 , 2, 28)	0.971 (37)	1.677

Continued on next page

Table 9: (Continued)

Line m	Line n	TW	Lit.	Line m	Line n	TW	Lit.
P(11, F_2 , 3, 39)	P(11, F_1 , 1, 43)	0.0	0.280	R(7, F_1 , 2, 29)	R(7, F_2 , 1, 29)	1.332 (61)	0.905
P(11, F_1 , 2, 42)	P(11, F_2 , 2, 40)	0.0	0.341	R(7, F_2 , 2, 28)	R(7, F_1 , 1, 30)	0.074 (34)	0.162
P(11, F_1 , 2, 42)	P(11, F_2 , 1, 41)	0.0	0.472	R(7, F_2 , 1, 29)	R(7, F_1 , 1, 30)	0.130 (8)	0.048
P(11, F_1 , 2, 42)	P(11, F_1 , 1, 43)	0.0	0.002	R(8, F_2 , 2, 33)	R(8, F_1 , 2, 31)	1.805 (67)	2.357
P(11, F_2 , 2, 40)	P(11, F_2 , 1, 41)	0.0	0.007	R(8, F_2 , 2, 33)	R(8, F_2 , 1, 34)	0.0	0.005
P(11, F_2 , 2, 40)	P(11, F_1 , 1, 43)	0.0	0.028	R(8, F_2 , 2, 33)	R(8, F_1 , 1, 32)	0.0	0.335
P(11, F_2 , 1, 41)	P(11, F_1 , 1, 43)	0.0	0.002	R(8, F_1 , 2, 31)	R(8, F_2 , 1, 34)	0.146 (11)	0.083
P(10, F_2 , 3, 37)	P(10, F_1 , 2, 36)	1.946 (72)	2.721	R(8, F_1 , 2, 31)	R(8, F_1 , 1, 32)	0.0	0.047
P(10, F_1 , 2, 36)	P(10, F_1 , 1, 37)	0.0	0.075	R(8, F_2 , 1, 34)	R(8, F_1 , 1, 32)	0.657 (46)	0.136
P(10, F_1 , 2, 36)	P(10, F_2 , 2, 38)	0.376 (15)	0.198	R(8, E , 2, 21)	R(8, E , 1, 22)	0.945 (68)	1.100
P(10, F_1 , 1, 37)	P(10, F_2 , 2, 38)	0.266 (10)	0.192	R(9, A_2 , 1, 13)	R(9, A_1 , 1, 12)	2.201 (81)	2.773
P(10, F_1 , 1, 37)	P(10, F_2 , 1, 39)	0.199 (11)	0.097	R(9, F_2 , 2, 34)	R(9, F_1 , 3, 36)	1.857 (70)	2.035
P(10, A_1 , 1, 14)	P(10, A_2 , 1, 12)	1.159 (43)	0.756	R(9, F_2 , 2, 34)	R(9, F_1 , 2, 37)	0.862 (81)	0.454
P(9, A_2 , 1, 12)	P(9, A_1 , 1, 10)	1.926 (71)	2.918	R(9, F_1 , 3, 36)	R(9, F_1 , 2, 37)	0.080 (65)	0.037
P(9, F_2 , 2, 32)	P(9, F_1 , 3, 33)	1.516 (56)	2.142	R(9, F_1 , 2, 37)	R(9, F_2 , 1, 35)	1.108 (41)	0.157
P(9, F_2 , 2, 32)	P(9, F_1 , 2, 34)	0.0	0.477	R(9, F_2 , 1, 35)	R(9, F_1 , 1, 38)	0.884 (43)	0.007
P(9, F_1 , 2, 34)	P(9, F_2 , 1, 33)	0.541 (20)	0.166	R(10, A_1 , 1, 14)	R(10, A_2 , 1, 12)	0.992 (63)	0.655
P(9, F_2 , 1, 33)	P(9, F_1 , 1, 35)	0.026 (5)	0.007	R(10, F_2 , 3, 39)	R(10, F_1 , 2, 38)	1.196 (46)	2.358
P(8, F_2 , 2, 30)	P(8, F_1 , 2, 28)	1.588 (59)	2.111	R(10, F_2 , 3, 39)	R(10, F_1 , 1, 39)	2.756 (100)	0.721
P(8, F_2 , 2, 30)	P(8, F_2 , 1, 31)	0.0	0.004	R(10, F_1 , 2, 38)	R(10, F_2 , 2, 40)	0.307 (25)	0.171
P(8, F_1 , 2, 28)	P(8, F_2 , 1, 31)	0.070 (12)	0.075	R(10, F_1 , 1, 39)	R(10, F_2 , 2, 40)	2.890 (110)	0.166
P(8, F_2 , 1, 31)	P(8, F_1 , 1, 29)	0.511 (21)	0.122	R(10, F_1 , 1, 39)	R(10, F_2 , 1, 41)	2.986 (120)	0.084
P(8, E , 2, 19)	P(8, E , 1, 20)	0.0	0.986	R(11, F_1 , 3, 43)	R(11, F_2 , 3, 41)	2.260 (85)	2.396
P(7, F_1 , 2, 26)	P(7, F_2 , 2, 24)	1.151 (45)	1.391	R(11, F_1 , 3, 43)	R(11, F_2 , 2, 42)	3.443 (150)	0.242
P(7, F_1 , 2, 26)	P(7, F_2 , 1, 25)	0.0	0.750	R(11, F_2 , 3, 41)	R(11, F_1 , 2, 42)	1.033 (42)	0.047
P(7, F_1 , 2, 26)	P(7, F_1 , 1, 27)	0.0	0.008	R(11, F_1 , 2, 42)	R(11, F_2 , 2, 42)	0.0	0.251
P(7, F_2 , 2, 24)	P(7, F_1 , 1, 25)	0.200 (140)	0.086	R(11, F_2 , 2, 42)	R(11, F_1 , 1, 44)	1.936 (72)	0.021
P(7, F_2 , 2, 24)	P(7, F_1 , 1, 27)	0.440 (160)	0.135	R(11, F_1 , 1, 43)	R(11, F_1 , 1, 44)	4.236 (160)	0.001
P(7, F_2 , 1, 25)	P(7, F_1 , 1, 27)	0.050 (16)	0.040	R(12, A_1 , 2, 16)	R(12, A_2 , 1, 15)	3.807 (140)	2.532
P(6, A_1 , 1, 8)	P(6, A_2 , 1, 6)	1.412 (52)	1.878	R(12, A_2 , 1, 15)	R(12, A_1 , 1, 17)	1.979 (75)	0.175
P(6, F_1 , 1, 21)	P(6, F_2 , 2, 22)	0.768 (28)	1.172	R(12, F_1 , 3, 45)	R(12, F_2 , 3, 48)	0.0	2.154
P(6, F_2 , 2, 22)	P(6, F_2 , 1, 23)	0.057 (9)	0.066	R(12, F_1 , 3, 45)	R(12, F_2 , 2, 46)	3.320 (150)	0.237
P(5, F_1 , 2, 18)	P(5, F_2 , 1, 17)	0.820 (30)	1.150	R(12, F_2 , 3, 48)	R(12, F_2 , 2, 46)	1.881 (99)	0.016
P(5, F_2 , 1, 17)	P(5, F_1 , 1, 19)	0.013 (2)	0.062				
P(4, F_2 , 1, 15)	P(4, F_1 , 1, 13)	0.364 (13)	0.566				
P(3, F_2 , 1, 9)	P(3, F_1 , 1, 11)	0.264 (10)	0.567				
Q(12, A_2 , 1, 17)	Q(12, A_1 , 2, 15)	3.217 (120)	1.540				
Q(12, F_2 , 3, 46)	Q(12, F_1 , 3, 47)	1.706 (64)					
Q(11, F_1 , 1, 40)	Q(11, F_2 , 1, 42)	1.776 (74)	0.001				
Q(11, F_1 , 2, 41)	Q(11, F_2 , 3, 44)	0.287 (100)	0.026				
Q(11, F_1 , 2, 41)	Q(11, F_1 , 3, 42)	0.667 (210)	0.001				
Q(11, F_2 , 3, 44)	Q(11, F_1 , 3, 42)	2.060 (130)	1.324				
Q(10, F_2 , 2, 37)	Q(10, F_1 , 1, 39)	0.263 (12)	0.075				
Q(10, F_1 , 2, 40)	Q(10, F_2 , 3, 38)	1.862 (69)	1.058				
Q(10, A_2 , 1, 14)	Q(10, A_1 , 1, 13)	0.0	0.294				
Q(9, F_1 , 1, 33)	Q(9, F_2 , 1, 35)	0.244 (14)	0.003				
Q(9, F_1 , 3, 35)	Q(9, F_2 , 2, 36)	1.267 (48)	0.927				
Q(8, F_2 , 1, 30)	Q(8, F_1 , 2, 32)	0.019 (6)	0.035				
Q(8, F_1 , 2, 32)	Q(8, F_2 , 2, 31)	0.435 (19)	0.998				
Q(8, E , 1, 21)	Q(8, E , 2, 22)	3.169 (130)	0.466				
Q(9, A_1 , 1, 13)	Q(9, A_2 , 1, 11)	1.262 (47)	1.263				
Q(7, F_1 , 1, 26)	Q(7, F_2 , 1, 28)	0.061 (11)	0.019				
Q(7, F_2 , 2, 29)	Q(7, F_1 , 2, 27)	1.091 (40)	0.661				
Q(6, F_2 , 2, 23)	Q(6, F_1 , 1, 25)	0.940 (35)	0.586				
Q(5, F_1 , 1, 19)	Q(5, F_2 , 1, 21)	0.266 (11)	0.037				
Q(5, F_2 , 1, 21)	Q(5, F_1 , 2, 20)	1.360 (51)	0.696				
Q(4, F_1 , 1, 17)	Q(4, F_2 , 1, 16)	1.248 (46)	0.473				
Q(3, F_1 , 1, 12)	Q(4, F_2 , 1, 16)	0.322 (13)	0.052				
Q(3, F_1 , 1, 12)	Q(3, F_2 , 1, 14)	0.584 (22)	0.466				
Q(2, F_2 , 1, 8)	Q(3, F_2 , 1, 14)	0.425 (16)	0.176				

Continued on next page

Table 9: (Continued)

Line m	Line n	TW	Lit.	Line m	Line n	TW	Lit.
Q(1, F_1 , 1, 5)	Q(2, F_2 , 1, 8)	0.029 (5)	0.373				

With the signal to noise ratio characterizing the spectra analyzed in the present work, it was noticed that the Rosenkranz approximation failed when the manifold included an off-diagonal coefficient larger than about $0.015 \text{ cm}^{-1}\text{atm}^{-1}$. As in previous work [24, 56], line-mixing between $A_1 \leftrightarrow A_1$, $A_2 \leftrightarrow A_2$, $F_1 \leftrightarrow F_1$ and $F_2 \leftrightarrow F_2$ was observed to be smaller than for the other allowed transitions. However, the off-diagonal coefficient is not negligible when the coupled lines are very close. The two coupled R(12) lines of F_2 symmetry are an example of such a case.

Table 9 also lists the values calculated for CH_4 -air in [75], multiplied by 1.3 as done in [11]. The qualitative agreement between the measured and calculated values is quite good in the P and R (up to $J'' = 9$) branches, although a few significant discrepancies are observed. The agreement is in contrast poorer in the Q branch and manifolds of the R branch with $J'' \geq 10$. In Table 10, the present measurements are compared with 1.3 times the off-diagonal relaxation matrix coefficients measured in the Q branch of the ν_3 band of CH_4 perturbed by air [76] or N_2 [37]. The corresponding calculated values [75] are also listed. It is interesting to note that the agreement

Table 10: Off-diagonal relaxation matrix coefficients W_{mn} (in $10^{-2} \text{ cm}^{-1}\text{atm}^{-1}$) for the ν_3 band of $^{12}\text{CH}_4$ perturbed by CO_2 measured in the present work (TW) and 1.3 times the values measured [76] or calculated [75] for CH_4 -air and measured for CH_4 - N_2 [37] ([0, 2d, 2] model).

Line m	Line n	TW	[76]	[37]	[75]
Q(12, F_2 , 3, 46)	Q(12, F_1 , 3, 47)	1.706 (64)	2.311 (25)	2.499 (25)	
Q(12, A_2 , 1, 17)	Q(12, A_1 , 2, 15)	3.217 (120)	3.556 (59)	3.331 (51)	1.540
Q(11, F_2 , 3, 44)	Q(11, F_1 , 3, 42)	2.060 (130)	3.700 (47)	3.238 (36)	1.324
Q(10, F_2 , 2, 37) [†]	Q(10, F_1 , 1, 39)	0.263 (12)	0.332 (15)	0.213 (13)	0.075
Q(10, F_1 , 2, 40)	Q(10, F_2 , 3, 38) [†]	1.862 (69)	2.332 (42)	2.112 (26)	1.058
Q(9, F_1 , 3, 35)	Q(9, F_2 , 2, 36)	1.267 (48)	1.881 (22)	1.913 (14)	0.927
Q(7, F_2 , 2, 29)	Q(7, F_1 , 2, 27)	1.091 (40)	0.855 (20)	0.856 (13)	0.661
Q(6, F_2 , 2, 23)	Q(6, F_1 , 1, 25)	0.940 (35)	1.533 (14)	1.515 (12)	0.586
Q(5, F_1 , 1, 19)	Q(5, F_2 , 1, 21)	0.266 (11)	0.495 (13)	0.415 (11)	0.037
Q(3, F_1 , 1, 12)	Q(3, F_2 , 1, 14)	0.584 (22)	0.402 (9)	0.331 (8)	0.466
Q(2, F_2 , 1, 8)	Q(1, F_1 , 1, 5)	0.029 (4)	0.564 (13)	0.354 (11)	0.373

[†] In [76], $\alpha' = 39$ (line m) and $\alpha'' = 1$ (line n). The assignments provided here are from the HITRAN database [22].

between the measurements is generally better than with the calculated values. Deviations between measured and calculated values are more apparent as J increases, the present measurements being systematically higher than Tran *et al.* [75] (with one exception) and lower than the measurements [37, 76] (with two exceptions). These coefficients often result from different couplings so there is less reliability in these comparisons. This is a recurring problem [37], which highlights the issue of whether these parameters have a physical meaning or are just effective.

Figure 14 presents a room temperature spectrum of the ν_3 band of CH_4 mixed with CO_2 at a total pressure of about 12.5 bars, recorded previously [11]. Spectra calculated using the relaxation

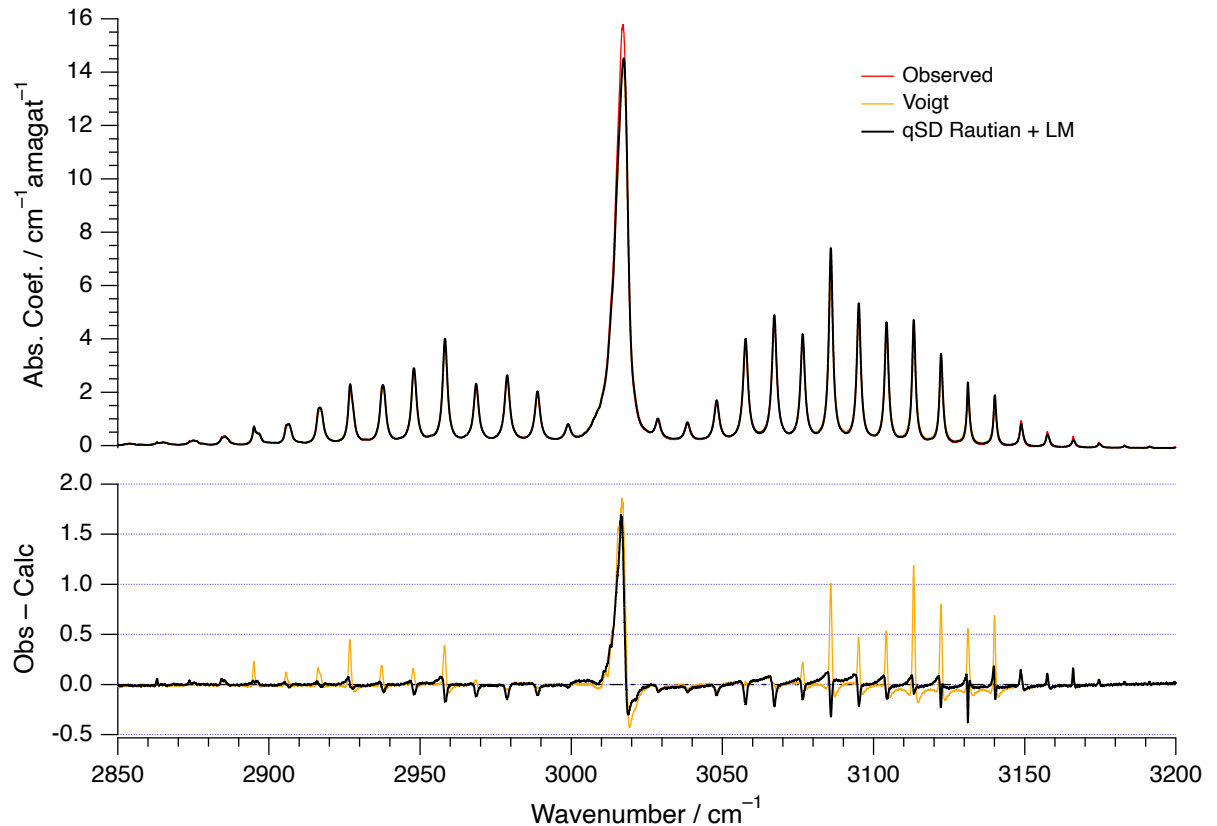


Figure 14: Comparison between a spectrum of the ν_3 band of CH_4 mixed with CO_2 at a total pressure of about 12.5 bars, recorded at room temperature (spectrum no. 2 in Table 1 of [11], red trace in the upper panel), and spectra calculated with the Voigt profile and neglecting line mixing effects (orange trace) and using the relaxation matrix formalism with all the parameters obtained in the present work (black trace). The corresponding residuals are presented in the lower panel. “qSD” and “LM” stand for “quadratic speed dependent” and “line mixing,” respectively.

matrix formalism and the quadratic speed dependent Rautian profile with all the parameters obtained in the present work as well as using the Voigt profile and neglecting line mixing effects (called “Voigt calculation” here after) are also presented. Note that these calculations and the two mentioned here below actually involved fitting the 5 coefficients of the 4th order polynomial expansion used to model the baseline of the spectra and the mole fraction of methane. As noted in [11], the fitted methane mole fraction was about 13 % lower than the value at cell filling. If the residuals obtained considering line mixing are similar to those presented in Fig. 3 of [11] for the P and R branches, they are close to those obtained with the Voigt calculation for the Q branch. Figure 15 focuses on this Q branch. In addition to the spectra presented in Fig. 14, it includes two spectra calculated using the relaxation matrix formalism with the line parameters of the present work and 1.3 times some of the off-diagonal relaxation matrix elements reported for CH₄-air [75] (all possible couplings in the ν_3 band are actually considered in this work), as done in [11]. Both calculations

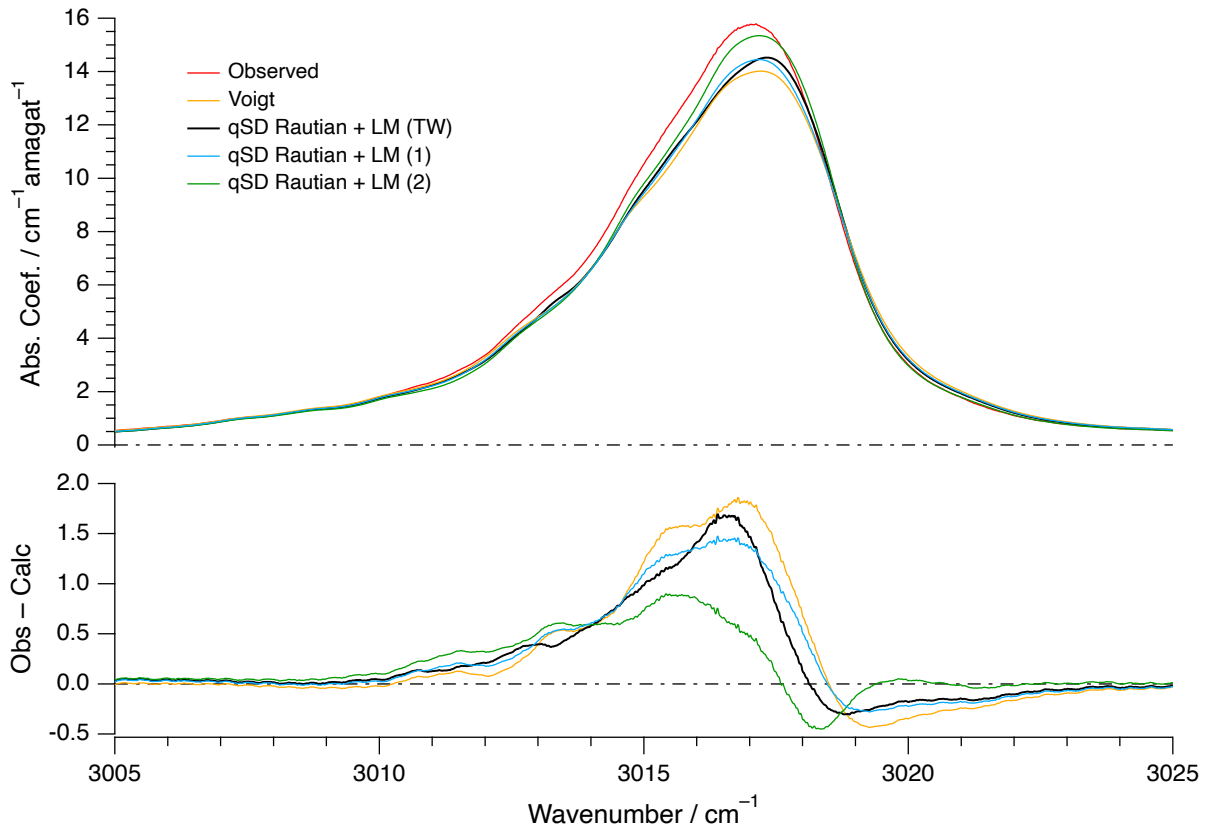


Figure 15: Same as Fig. 14, focusing on the Q branch of the ν_3 band of CH₄ (“qSD” and “LM” stand for “quadratic speed dependent” and “line mixing,” respectively). The additional two spectra [identified by (1) and (2)] and their corresponding residuals were calculated using the relaxation matrix formalism with the line parameters obtained in the present work and the values of the off-diagonal relaxation matrix elements reported in [75], multiplied by 1.3 as done in [11]: the blue traces were generated neglecting all inter- J and inter-branch couplings, while the green traces were calculated considering $\Delta J = \pm 1$ couplings. Both calculations included $\Delta J = 0$ couplings.

include the $\Delta J = 0$ couplings. The blue traces correspond to the spectrum generated neglecting all inter- J and inter-branch couplings, while the green traces were obtained also considering $\Delta J = \pm 1$ couplings. These two calculations show the importance of the $\Delta J = \pm 1$ couplings in the Q branch.

Not considering them beyond $J'' = 4$ (see section 3) therefore reduced the applicability to higher pressures of the parameters retrieved for the Q branch in the present work.

First order line mixing coefficients Y_n^0 , calculated using Eq. 10, are also listed in Table 7. These calculated values agree within 20 % with 44 of the 62 coefficients measured for P(12) to R(7). Significantly poorer agreement is observed for the more congested R(8) to R(12) manifolds, matching the emergence of signatures in the residuals of Figs. 3 and 5, however one J'' higher. Inspection of the last column of Table 7 indicates that poorer agreement between observed and calculated values can also be attributed to missing measured off-diagonal relaxation matrix elements.

6. Conclusion

CO_2 broadening and shift coefficients together with speed dependence of the broadening have been measured for lines belonging to J'' manifolds of the P ($J'' = 1 - 13$), Q ($J'' = 1 - 13$) and R ($J'' = 0 - 13$) branches of the ν_3 band of $^{12}\text{CH}_4$ observed near 3.3 μm . The CO_2 shift coefficients are reprotoed for the first time. These measurements were carried out using non-linear multispectrum least squares fitting techniques, applied to eleven high resolution Fourier transform spectra recorded at 296.5 (5) K. These consisted in one spectrum of pure methane at low pressure and 10 spectra of mixtures of methane and carbon dioxide at total pressures between 26 and 803 hPa. Methane lines were modeled using a hard collision speed dependent Rautian line shape model. This line shape model was chosen because it was found necessary to fit the observed shape of the $R(0, A_1, 1, 3)$ and $R(1, F_1, 1, 10)$ lines to the noise level. Although Dicke narrowing was included in the analyses, the measured Dicke narrowing coefficients were rather small and involved a possible correlation with the speed dependence of broadening. These observations were interpreted as an indication that the present measurements did not rely on enough spectra corresponding to total pressures below about 200 hPa. The measured narrowing coefficients were therefore not reported. As already reported in the literature for methane and other molecules [37, 65–69], the speed dependence of broadening coefficients is on average equal to about $a_w = 0.110$. Apart from the CO_2 broadening coefficients that exhibit a dependence on the tetrahedral symmetries already observed for other perturber gases, such a dependence was not observed for the other parameters measured in the present work.

Line mixing was considered in the analyses using the first order in pressure approximation or the relaxation matrix formalism. The work carried out demonstrated that first order line mixing can be sufficient to model absorption spectra of manifolds involving a low density of lines at total pressures up to 800 hPa. As J increases, the density of lines in the manifolds increases and signatures indicating the failure of the first order approximation appear in the residuals. The use of the relaxation matrix formalism allowed bringing the residuals to the noise level. It however failed in the low J part of the Q branch near 3020 cm^{-1} . More line couplings or a hybrid relaxation matrix / first order model accounting would probably be needed to be solve this problem.

Prior to the present work, limited information was available in the literature on parameters characterizing the effects of the pressure of CO_2 on the absorption spectrum of the ν_3 band of $^{12}\text{CH}_4$. Differences between the values of the parameters reported in the literature and measured in this work do not generally show any systematic discrepancies.

Supplementary material

The supplementary material provided with this article consists in two files listing the CO_2 -induced collisional line parameters measured at 296.5 (5) K for the ν_3 band of $^{12}\text{CH}_4$ in fits F1 and

F4 of this work.

Acknowledgments

T. Bertin thanks the *Fonds pour la formation à la Recherche dans l'Industrie et dans l'Agriculture* (FRIA, Belgium) for a PhD fellowship. This work was financially supported by the *Fonds de la Recherche Scientifique*–FNRS (Belgium, contract J.0217.20).

References

- [1] Canadell J, Scheel Monteiro P, Costa M, Cotrim Da Cunha L, Cox PM, Eliseev AV, Henson S, Ishii M, Jaccard S, Koven C, Lohila A, Patra P, Piao S, Rogelj J, Syampungani S, Zaehle S, Zickfeld K, Brovkin V, Feely R. Global carbon and other biogeochemical cycles and feedbacks. Climate change 2021: the physical science basis. Working group I contribution to the sixth assessment report of the intergovernmental panel on climate change. Masson-Delmotte V, Zhai P, Pirani A, Connors SL, Péan C, Berger S, Caud N, Chen Y, Goldfarb L, Gomis MI, Huang M, Leitzell K, Lonnoy E, Matthews JBR, Maycock TK, Waterfield T, Yelekçi O, Yu R, Zhou B, editors. Cambridge, United Kingdom and New York, NY, USA: Cambridge University Press, 2021. doi:10.1017/9781009157896
- [2] Sinclair JA, Orton GS, Fletcher LN, Roman M, de Pater I, Encrenaz T, Hammel HB, Giles RS, Velusamy T, Moses JI, Irwin PGJ, Momary TW, Rowe-Gurney N, Tabataba-Vakili F. Spatial structure in Neptune's 7.90 μm stratospheric CH₄ emission, as measured by VLT-VISIR. Icarus 2020;345:113748. doi:10.1016/j.icarus.2020.113748
- [3] Sánchez-López A, López-Puertas M, García-Comas M, Funke B, Fouchet T, Snellen IAG. The CH₄ abundance in Jupiter's upper atmosphere. Astron Astrophys 2022;662:A91. doi:10.1051/0004-6361/202141933
- [4] Dinelli BM, López-Puertas M, Fabiano F, Adriani A, Moriconi ML, Funke B, García-Comas M, Oliva F, D'Aversa E, Filacchione G. Climatology of CH₄, HCN and C₂H₂ in Titan's upper atmosphere from Cassini/VIMS observations. Icarus 2019;331:83–97. doi:10.1016/j.icarus.2019.04.026
- [5] Swain MR, Vasisht G, Tinetti G. The presence of methane in the atmosphere of an extrasolar planet. Nature 2008;452:329–31. doi:10.1038/nature06823
- [6] Macintosh B, Graham JR, Barman T, De Rosa RJ, Konopacki Q, Marley MS, Marois C, Nielsen EL, Pueyo L, Rajan A, Rameau J, Saumon D, Wang JJ, Patience J, Ammons M, Arriaga P, Artigau E, Beckwith S, Brewster J, Bruzzone S, Bulger J, Birmingham B, Burrows AS, Chen C, Chiang E, Chilcote JK, Dawson RI, Dong R, Fitzgerald MP, Follette KB, Fortney JJ, Gerard B, Goodsell S, Greenbaum AZ, Hibon P, Hinkley S, Cotten TH, Hung LW, Ingraham P, Johnson-Groh M, Kalas P, Lafreniere D, Larkin JE, Lee J, Line M, Long D, Maire J, Marchis F, Matthews BC, Max CE, Metchev S, Millar-Blanchaer MA, Mittal T, Morley CV, Morzinski KM, Murray-Clay R, Oppenheimer R, Palmer DW, Patel R, Perrin MD, Poyneer LA, Rafikov RR, Rantakyrö FT, Rice EL, Rojo P, Rudy AR, Ruffio JB, Ruiz MT, Sadakuni N, Saddlemyer L, Salana M, Savransky D, Schneider AC, Sivaramakrishnan A, Song I, Soummer R, Thomas S, Vasisht G, Wallace JK, Ward-Duong K, Wiktorowicz SJ, Wolff SG, Zuckerman B. Discovery and spectroscopy of the young jovian planet 51 Eri b with the Gemini Planet Imager. Science 2015;350:64–7. doi:10.1126/science.aac5891
- [7] Swain MR, Esstrela R, Roudier GM, Sotin C, Rimmer PB, Valio A, West R, Pearson K, Huber-Feely N, Zellem RT. Detection of an atmosphere on a rocky exoplanet. ApJ 2021;161:213. doi:10.3847/1538-3881/abe879
- [8] Grenfell JL, Wunderlich F, Sinnhuber M, Herbst K, Lehmann R, Scheucher M, Gebauer S, Arnold G, Rauer H. Atmospheric processes affecting methane on Mars. Icarus 2002;382:114940. doi:10.1016/j.icarus.2002.114940
- [9] Wordsworth S, Kalugina Y, Lokshtanov S, Vigasin A, Ehlmann B, Head J, Sanders C, Wang H. Transient reducing greenhouse warming on early Mars. Geophys Res Lett 2017;44:665–71. doi:10.1002/2016GL071766
- [10] Turret M, Tran H, Pirali O, Forget F, Boulet C, Hartmann JM. Far infrared measurements of absorptions by CH₄ + CO₂ and H₂ + CO₂ mixtures and implications for greenhouse warming of early Mars. Icarus 2019;321:189–99. doi:10.1016/j.icarus.2018.11.021
- [11] Tran H, Vander Auwera J, Bertin T, Fakhadjji W, Pirali O, Hartmann JM. Absorption of methane broadened by carbon dioxide in the 3.3 μm spectral region: From line centers to the far wings. Icarus 2022;384:115093. doi:10.1016/j.icarus.2022.115093
- [12] Es-sebbar E, Farooq A. Line-strengths, collisional coefficients and narrowing parameters in the ν_3 band of methane: H₂, He, N₂, O₂, Ar and CO₂ collider effects. J Quant Spectrosc Radiat Transf 2021;272:107758. doi:10.1016/j.jqsrt.2021.107758

[13] Gharavi M, Buckley SG. Diode laser absorption spectroscopy measurement of linestrengths and pressure broadening coefficients of the methane $2\nu_3$ band at elevated temperatures. *J Mol Spectrosc* 2005;229:78–88. doi:10.1016/j.jms.2004.07.016

[14] Lyulin O, Petrova T, Solodov A, Solodov A, Perevalov V. Measurements of the broadening and shift parameters of methane spectral lines in the 5550–6140 cm^{-1} region induced by pressure of carbon dioxide. *J Quant Spectrosc Radiat Transf* 2014;147:164–70. doi:10.1016/j.jqsrt.2014.05.027

[15] Fissiaux L, Delière Q, Blanquet G, Robert S, Vandaele AC, Lepère M. CO_2 -broadening coefficients in the ν_4 fundamental band of methane at room temperature and application to CO_2 -rich planetary atmospheres. *J Mol Spectrosc* 2014;297:35–40. doi:10.1016/j.jms.2014.01.006

[16] Vispoel B, Fissiaux L, Lepère M. CO_2 -broadening coefficients in the ν_3 fundamental band of methane. *J Mol Spectrosc* 2019;360:1–6. doi:10.1016/j.jms.2018.12.004

[17] Es-sebbar E, Farooq A. Intensities, broadening and narrowing parameters in the ν_3 band of methane. *J Quant Spectrosc Radiat Transf* 2014;149:241–52. doi:10.1016/j.jqsrt.2014.08.008

[18] Manne J, Bui TQ, Webster CR. Determination of foreign broadening coefficients for methane lines targeted by the tunable laser spectrometer (TLS) on the Mars Curiosity rover. *J Quant Spectrosc Radiat Transf* 2017;191:59–66. doi:10.1016/j.jqsrt.2017.01.035

[19] Koroglu B, Neupane S, Pryor O, Peale RE, Vasu SS. High temperature infrared absorption cross sections of methane near 3.4 μm in Ar and CO_2 mixtures. *J Quant Spectrosc Radiat Transf* 2018;206:36–45. doi:10.1016/j.jqsrt.2017.11.003

[20] Dicke RH. The Effect of collisions upon the Doppler width of spectral lines. *Phys Rev* 1953;89:472–3. doi:10.1103/PhysRev.89.472

[21] Rosenkranz P. Shape of the 5 mm oxygen band in the atmosphere. *IEEE Trans Anten Propag* 1975;23:498–506. doi:10.1109/TAP.1975.1141119

[22] Gordon IE, Rothman LS, Hargreaves RJ, Hashemi R, Karlovets EV, Skinner FM, Conway EK, Hill C, Kochanov RV, Tan Y, Wcislo P, Finenko AA, Nelson K, Bernath PF, Birk M, Boudon V, Campargue A, Chance KV, Coustenis A, Drouin BJ, Flaud JM, Gamache RR, Hodges JT, Jacquemart D, Mlawer EJ, Nikitin AV, Perevalov VI, Rotger M, Tennyson J, Toon GC, Tran H, Tyuterev VG, Adkins EM, Baker A, Barbe A, Canè E, Császár AG, Dudaryonok A, Egorov O, Fleisher AJ, Fleurbaey H, Foltynowicz A, Furtenbacher T, Harrison JJ, Hartmann JM, Horneman VM, Huang X, Karman T, Karns J, Kassi S, Kleiner I, Kofman V, Kwabia Tchana F, Lavrentieva NN, Lee TJ, Long DA, Lukashevskaya AA, Lyulin OM, Makhnev VY, Matt W, Massie ST, Melosso M, Mikhailenko SM, Mondelain D, Müller HSP, Naumenko OV, Perrin A, Polyansky OL, Raddaoui E, Raston PL, Reed ZD, Rey M, Richard C, Tóbiás R, Sadiek I, Schwenke DW, Starikova E, Sung K, Tamassia F, Tashkun SA, Vander Auwera J, Vasilenko IA, Vigasin AA, Villanueva GL, Vispoel B, Wagner G, Yachmenev A, Yurchenko SN. The HITRAN2020 molecular spectroscopic database. *J Quant Spectrosc Radiat Transf* 277 (2022) 107949. doi:10.1016/j.jqsrt.2021.107949

[23] Baranger M. Problem of overlapping lines in the theory of pressure broadening. *Phys Rev* 1958;111:494–504. doi:10.1103/PhysRev.111.494

[24] Farji A, Aroui H, Vander Auwera J. Air-induced collisional parameters in the ν_3 band of methane. *J Quant Spectrosc Radiat Transf* 2021;275:107878. doi:10.1016/j.jqsrt.2021.107878

[25] Fano U. Pressure broadening as a prototype of relaxation. *Phys Rev* 1963;131:259–68. doi:10.1103/PhysRev.131.259

[26] Lévy A, Lacome N, Chackerian C Jr. Collisional line mixing. In *Spectroscopy of the Earth atmosphere and interstellar medium*. Academic Press, New York. pp. 261–337. 1992.

[27] Ciurylo R, Pine AS. Speed-dependent line mixing profiles. *J Quant Spectrosc Radiat Transf* 2000;67:375–93. doi:10.1016/S0022-4073(00)00030-3

[28] Cacciani P, Čermák P, Vander Auwera J, Campargue A. The ammonia absorption spectrum between 3900 and 4700 cm^{-1} . *J Quant Spectrosc Radiat Transf* 2022;277:107961. doi:10.1016/j.jqsrt.2021.107961

[29] Bertin T, Vander Auwera J. A python software to retrieve the instrument line shape of a Fourier transform spectrometer. In preparation.

[30] Hase F, Blumenstock T, Paton-Walsh C. Analysis of the instrument line shape of high-resolution Fourier transform IR spectrometers with gas cell measurements and new retrieval software. *Appl Opt* 1999;38:3417–22. doi:10.1364/AO.38.003417

[31] Boone CD, Bernath PF. The instrument line shape of the atmospheric chemistry experiment Fourier transform spectrometer (ACE-FTS). *J Quant Spectrosc Radiat Transf* 2019;230:1–12. doi:10.1016/j.jqsrt.2019.03.018

[32] Bunker PR, Jensen P. Molecular symmetry and spectroscopy, 2nd edition, NRC Research Press, Ottawa, Ontario, Canada (2006).

[33] Brown LR, Margolis JS, Champion JP, Hilico JC, Jouvard JM, Loëte M, Chackerian C Jr, Tarrago G, Benner DC. Methane and its isotopes: Current status and prospects for improvement. *J Quant Spectrosc Radiat Transf* 1992;48:617–28. doi:10.1016/0022-4073(92)90126-O

[34] Hartmann JM, Boulet C, Robert D. Collisional effects on molecular spectra – Laboratory experiments and models, consequences for applications. Second edition. Elsevier, Amsterdam (2021). ISBN: 978-0-12-822364-2

[35] Gamache RR, Vispoel B, Rey M, Nikitin A, Tyuterev V, Egorov O, Gordon IE, Boudon V. Total internal partition sums for the HITRAN2020 database. *J Quant Spectrosc Radiat Transf* 2021;271:107713. doi:10.1016/j.jqsrt.2021.107713

[36] Lance B, Blanquet G, Walrand J, Bouanich JP. On the speed-dependent hard collision lineshape models: Application to C_2H_2 perturbed by Xe. *J Mol Spectrosc* 1997;185:262–71. doi:10.1006/jmsp.1997.7385

[37] Pine AS. Speed-dependent line mixing in the ν_3 band Q branch of methane. *J Quant Spectrosc Radiat Transf* 2019;224:62–77. doi:10.1016/j.jqsrt.2018.10.038

[38] Rohart F, Nguyen L, Buldyreva J, Colmont JM, Włodarczak G. Lineshapes of the 172 and 602 GHz rotational transitions of $HC^{15}N$. *J Mol Spectrosc* 2007;246:213–27. doi:10.1016/j.jms.2007.09.009

[39] Tran H, Ngo NH, Hartmann JM. Efficient computation of some speed-dependent isolated line profiles. *J Quant Spectrosc Radiat Transf* 2013;129:199–203. doi:10.1016/j.jqsrt.2013.06.015

[40] Schreier F, Gimeno García S, Hochstafl P, Städter S. Py4CatS – Python for computational atmospheric spectroscopy. *Atmosphere* 2019;10:262. doi:10.3390/atmos10050262

[41] Lisak D, Masłowski P, Cygan A, Bielska K, Wójtewicz S, Piwiński, Hodges JT, Trawiński, Ciuryło R. Line shapes and intensities of self-broadened O_2 $b^1\Sigma_g^+(v=1) \leftarrow X^3\Sigma_g^-(v=0)$ band transition measured by cavity ring-down spectroscopy. *Phys Rev A* 2010;81:042504.

[42] Kolb AC, Griem H. Theory of line broadening in multiplet spectra. *Phys Rev* 1958;111:514–21. doi:10.1103/PhysRev.111.514

[43] Ben-Reuven A. Impact broadening of microwave spectra. *Phys Rev* 1966;145:7–22. doi:10.1103/PhysRev.145.7

[44] Gordon RG. Semiclassical theory of spectra and relaxation in molecular gases. *J Chem Phys* 1966;45:1649–55. doi:10.1063/1.1727808

[45] Gordon RG, McGinnis RP. Intermolecular potentials and infrared spectra. *J Chem Phys* 1971;55:4898–906. doi:10.1063/1.1675597

[46] Lam KS. Application of pressure broadening theory to the calculation of atmospheric oxygen and water vapor microwave absorption. *J Quant Spectrosc Radiat Transf* 1977;17:351–83. doi:10.1016/0022-4073(77)90115-7

[47] Smith EW. Absorption and dispersion in the O_2 microwave spectrum at atmospheric pressures. *J Chem Phys* 1981;74:6658–73. doi:10.1063/1.441112

[48] Gentry B, Strow LL. Line mixing in a N_2 -broadened CO_2 Q branch observed with a tunable diode laser. *J Chem Phys* 1987;86:5722–30. doi:10.1063/1.452770

[49] Pine AS. Line mixing sum rules for the analysis of multiplet spectra. *J Quant Spectrosc Radiat Transf* 1997;57:145–55. doi:10.1016/S0022-4073(96)00129-X

[50] Pine AS. N_2 and Ar broadening and line mixing in the P and R branches of the ν_3 band of CH_4 . *J Quant Spectrosc Radiat Transf* 1997;57:157–76. doi:10.1016/S0022-4073(96)00130-6

[51] Rautian SG, Sobel'man II. The effect of collisions on the Doppler broadening of spectral lines. *Sov Phys Uspekhi* 1967;9:701–16. doi:10.1070/PU1967v009n05ABEH003212

[52] Tudorie M, Földes T, Vandaele AC, Vander Auwera J. CO_2 pressure broadening and shift coefficients for the $1 - 0$ band of HCl and DCl . *J Quant Spectrosc Radiat Transf* 2012;113:1092–101. doi:10.1016/j.jqsrt.2012.01.025

[53] Daneshvar L, Földes T, Buldyreva J, Vander Auwera J. Infrared absorption by pure CO_2 near 3340 cm^{-1} : measurements and analysis of collisional coefficients and line-mixing effects at subatmospheric pressures. *J Quant Spectrosc Radiat Transf* 2014;149:258–74. doi:10.1016/j.jqsrt.2014.08.007

[54] Virtanen P, Gommers R, Oliphant TE, Haberland M, Reddy T, Cournapeau D, Burovski E, Peterson P, Weckesser W, Bright J, van der Walt SJ, Brett M, Wilson J, Millman KJ, Mayorov N, Nelson ARJ, Jones E, Kern R, Larson E, Carey CJ, Polat İ, Feng Y, Moore EW, VanderPlas J, Laxalde D, Perktold J, Cimrman R, Henriksen I, Quintero EA, Harris CR, Archibald AM, Ribeiro AH, Pedregosa F, van Mulbregt P, SciPy 1.0 Contributors. SciPy 1.0: Fundamental algorithms for scientific computing in Python. *Nature Methods* 2020;17:261–272. doi:10.1038/s41592-019-0686-2

[55] Pieroni D, Van Thanh N, Brodbeck C, Claveau C, Valentin A, Hartmann JM, Gabard T, Champion JP, Bermejo D, Domenech JL. Experimental and theoretical study of line mixing in methane spectra. I. The N_2 -broadened ν_3 band at room temperature. *J Chem Phys* 1999;110:7717–32.

[56] Pine AS, Gabard T. Speed-dependent broadening and line mixing in CH_4 perturbed by Ar and N_2 from multispectrum fits. *J Quant Spectrosc Radiat Transf* 2000;66:69–92. doi:10.1016/S0022-4073(99)00222-8

[57] Abe M, Iwakuni K, Okubo S, Sasada H. Accurate transition frequency list of the ν_3 band of methane from sub-Doppler resolution comb-referenced spectroscopy. *J Opt Soc Am B* 2013;30:1027–35. doi:10.1364/JOSAB.30.001027

[58] Predoi-Cross A, Brown LR, Devi VM, Brawley-Tremblay M, Benner DC. Multispectrum analysis of $^{12}\text{CH}_4$ from 4100 to 4635 cm^{-1} : 1. Self-broadening coefficients (widths and shifts). *J Mol Spectrosc* 2005;232:231–46. doi:10.1016/j.jms.2005.04.007

[59] Lepère M. Self-broadening coefficients in the ν_4 band of CH_4 by diode-laser spectroscopy. *J Mol Spectrosc* 2006;238:193–9. doi:10.1016/j.jms.2006.05.002

[60] Smith MAH, Benner DC, Predoi-Cross A, Devi VM. Multispectrum analysis of $^{12}\text{CH}_4$ in the ν_4 spectral region: II. Self-broadened half widths, pressure-induced shifts, temperature dependences and line mixing. *J Quant Spectrosc Radiat Transf* 2010;111:1152–66. doi:10.1016/j.jqsrt.2010.01.017

[61] Lyulin OM, Perevalov VI, Morino I, Yokota T, Kumazawa R, Watanabe T. Measurements of self-broadening and self-pressure-induced shift parameters of the methane spectral lines in the 5556 – 6166 cm^{-1} range. *J Quant Spectrosc Radiat Transf* 2011;112:531–9. doi:10.1016/j.jqsrt.2010.10.010

[62] Smith MAH, Benner DC, Predoi-Cross A, Devi VM. Air- and self-broadened half widths, pressure-induced shifts, and line mixing in the ν_2 band of $^{12}\text{CH}_4$. *J Quant Spectrosc Radiat Transf* 2014;133:217–34. doi:10.1016/j.jqsrt.2013.08.004

[63] Hashemi R, Predoi-Cross A, Nikitin AV, Tyuterev VG, Sung K, Smith MAH, Devi VM. Spectroscopic line parameters of $^{12}\text{CH}_4$ for atmospheric composition retrievals in the 4300 – 4500 cm^{-1} region. *J Quant Spectrosc Radiat Transf* 2017;186:106–17. doi:10.1016/j.jqsrt.2016.03.024

[64] Mondelain D, Chelin P, Valentin A, Hurtmans D, Camy-Peyret C. Line profile study by diode laser spectroscopy in the $^{12}\text{CH}_4$ $\nu_2 + \nu_4$ band. *J Mol Spectrosc* 2005;233:23–31. doi:10.1016/j.jms.2005.05.012

[65] Devi VM, Benner DC, Sung K, Crawford TJ, Yu S, Brown LR, Smith MAH, Mantz AW, Boudon V, Ismail S. Self- and air-broadened line shapes in the $2\nu_3$ P and R branches of $^{12}\text{CH}_4$. *J Mol Spectrosc* 2015;315:114–36. doi:10.1016/j.jms.2015.05.003

[66] Devi VM, Benner DC, Smith MAH, Mantz AW, Sung K, Brown LR, Predoi-Cross A. Spectral line parameters including temperature dependences of self- and air-broadening in the $2 \leftarrow 0$ band of CO at 2.3 μm . *J Quant Spectrosc Radiat Transf* 2012;113:1013–33. doi:10.1016/j.jqsrt.2012.02.010

[67] Devi VM, Benner DC, Brown LR, Miller CE, Toth RA. Line mixing and speed dependence in CO_2 at 6348 cm^{-1} : Positions, intensities and air- and self-broadening derived with constrained multispectrum analysis. *J Mol Spectrosc* 2007;242:90–117. doi:10.1016/j.jms.2007.02.018

[68] Bui Tq, Long DA, Cygan A, Sironneau VT, Hogan DW, Rupasinghe PM, Ciurylo R, Lisak D, Okumura M. Observations of Dicke narrowing and speed dependence in air-broadened CO_2 lineshapes near 2.06 μm . *J Chem Phys* 2014;141:174301. doi:10.1063/1.4900502

[69] Okubo S, Iwakuni K, Kato H, Hong FL, Sasada H, Inaba H, Yamada KMT. The pressure effect on the line profiles observed in the $\nu_1 + \nu_3$ band of acetylene: Revisited. *J Mol Spectrosc* 2023;396:111823.

[70] Loos J, Birk M, Wagner G. Measurement of positions, intensities and self-broadening line shape parameters of H_2O lines in the spectral ranges 1850 – 2280 cm^{-1} and 2390 – 4000 cm^{-1} . *J Quant Spectrosc Radiat Transf* 2017;203:119–32. doi:10.1016/j.jqsrt.2017.02.013

[71] Ballard J, Johnston WB. Self-broadened widths and absolute strengths of $^{12}\text{CH}_4$ lines in the 1310 – 1370 cm^{-1} region. *J Quant Spectrosc Radiat Transf* 1986;36:365–71. doi:10.1016/0022-4073(86)90061-0

[72] Margolis JS. Measurement of hydrogen-broadened methane lines in the ν_4 band at 296 and 200 K. *J Quant Spectrosc Radiat Transf* 1993;50:431–41. doi:10.1016/0022-4073(93)90073-Q

[73] Gabard T. Argon-broadened line parameters in the ν_3 band of $^{12}\text{CH}_4$. *J Quant Spectrosc Radiat Transf* 1997;57:177–96. doi:10.1016/S0022-4073(96)00131-8

[74] Fox K, Jennings DE. Spectroscopic studies of methane in collisions with rare gas atoms and diatomic molecules. *J Mol Struct* 1990;224:1–6. doi:10.1016/0022-2860(90)87002-F

[75] Tran H, Flaud PM, Gabard T, Hase F, von Clarmann T, Camy-Peyret C, Payan S, Hartmann JM. Model, software and database for line-mixing effects in the ν_3 and ν_4 bands of CH_4 and tests using laboratory and planetary measurements – I: N_2 (and air) broadenings and the Earth atmosphere. *J Quant Spectrosc Radiat Transf* 2006;101:284–305. doi:10.1016/j.jqsrt.2005.11.020

[76] Devi VM, Benner DC, Gamache RR, Tran H, Smith MAH, Sams RL. Multispectrum analysis of air-broadened spectra in the ν_3 Q branch of $^{12}\text{CH}_4$. *J Quant Spectrosc Radiat Transf* 2018;206:409–29. doi:10.1016/j.jqsrt.2017.12.005